UNIVERSITY OF OSLO
Department of Physics

Time dynamic channel model for broadband fixed wireless access systems

Master thesis

Michael Cheffena

May 2005

Time dynamic channel model for broadband fixed wireless access systems

By
Michael Cheffena

Preface

This master thesis focuses on the time varying broadband fixed wireless access channel and development of a realistic time dynamic channel model for systems operating above 20 GHz. Telenor R&D, located at Fornebu, Oslo, awarded the thesis. The research was conducted at Telenor R&D under the supervision of Dr. Ing. Lars Erling Bråten (internal supervisor) and Dr. Pål Orten (main supervisor). I start writing my master thesis on the 17 of January 2005, and finished on the 30 of May 2005. I am grateful to my supervisor Lars Erling Bråten for his guidance and for the opportunity he gave me to carry out this work. Also, I would like to thank Terje Telta, Magene pettersen and Pål Orten for their help and guidance. I would like to thank my friend David O. A. Ojelade and the staff and researches of Telenor R&D for their help and co-operation.

Abstract

Broadband fixed wireless access (BFWA) systems have been recognized as an effective first kilometer solution for broadband services to residential and business customers. The large bandwidth available in frequency bands above 20 GHz makes radio systems with very high capacities possible. Users can be offered bit rates in the order of several hundred Mbit/s, making (in terms of capacity) such radio links an alternative to optical fibre in many cases. High capacities BFWA links can be used to serve individual users directly or function as a backbone for lower capacity systems (both wire line and wireless) for local distribution of data. In addition, wireless always offers the freedom of broadband being away from the fixed access point.

At mm-wavelengths the signals are sensitive to time dynamic propagation degradation caused by precipitation, vegetation and reflections/multipath from e.g. building surfaces. BFWA need to cope with location and time dependent interference and employ techniques such as interference cancellation and adaptive modulation and coding to optimise throughput during varying traffic load conditions. Multiple input multiple output (MIMO) and space-time coding, as well as adaptive (smart) antennas require knowledge of the channel dynamics as well.

The objective of this master thesis is to develop a realistic time dynamic channel model for BFWA operating above 20 GHz utilising adaptive physical layer techniques. The channel model developed represents the time varying wideband channel impulse response including degradations due to multipath propagation, rain attenuation and vegetation fading. The channel model is suitable for simulating mitigation techniques for interference between base stations as well as adaptive modulation and coding techniques.

The Maseng-Bakken statistical dynamic model of rain attenuation was adapted to model the rain attenuation. The dynamic vegetation effect was modelled as Nakagami-Rice distribution with K-factor depending on wind speed. A generic tapped delay line model was developed, in which the number of taps depend on maximum tap delay.

This thesis is based on work in the project BROADWAN (www.broadwan.org), partly funded under the Information Society Technologies (IST) priority of the European Commission Sixth Framework Program.

Table of Contents

1 Introduction

BFWA may be divided between systems that operate below 20 GHz and systems that operate above 20 GHz. For systems operating above 20 GHz, there is available wide bandwidth for delivering broadband services such as video, audio and data. In addition, a high frequency reuse is possible, and the size of radiating and receiving antennas and electronic components is reduced compared to lower frequency systems. However, millimetre-wave signals are more sensitive to propagation degradation due to rain and vegetation; in addition the wideband signals are susceptible to frequency selective fading due to multipath propagation. Thus a realistic channel model that accounts the effect of rain, vegetation and multipath is necessary for simulation interference mitigation and capacity enhancing techniques. In this thesis we focus on high capacity BFWA operating above 20 GHz, and develop a time dynamic channel model suitable for simulating capacity enhancing and interference mitigation techniques.

Based on measurements conducted at 27.4 GHz, static and dynamic wideband channel model for BFWA were developed [1]. Dynamic models for rain attenuation are reported in for example [2] and [3]. There are a number of studies on the dynamic effects of vegetation among them [4] and [5]. Different wideband and narrowband measurements between 20 to 50 GHz have been studied in order to understand both the wideband and the narrowband effects of BFWA channel, these measurement results are discussed in detail in Section 5. This thesis presents a wideband statistical channel model, which combines the effect of precipitation, vegetation and multipath propagation.

The report is outlined as follows, Section 2 introduces existing broadband technologies, and concentrates on BFWA systems operating above 20 GHz, sometimes denoted Local Multipoint Distribution Service (LMDS). In addition this section provides some information about BFWA architecture. In Section 3 some basic radio wave propagation mechanisms are discussed in the context of time varying broadband fading channels. Section 4 describes the communication system considered for the development of the channel model. Section 5 discusses wideband and narrowband measurements and results describing vegetation, rain, and multipath effects. In addition this section discusses existing dynamic rain and vegetation attenuation models, and tapped delay line multipath models. Section 6 presents the proposed time dynamic channel model for BFWA systems operating above 20 GHz, taking into accounts the effect of rain, vegetation and multipath. Section 7 concludes the conducted study and gives suggestion for future works. Appendix A presents a paper resulting from this work, the paper will be published and presented at 3rd international workshop in COST Action 280, Propagation Impairments Mitigation for Millimeter-Wave Radio Systems 6th - 8th June 2005, Prague, Czech Republic.

2 Broadband access technologies

At present there are different broadband technologies employed. Examples include digital subscriber link (DSL) technologies deliver broadband services through telephone copper wire line, hybrid fibre coaxial (HFC) network, fibre-to-the home (FTTH), power line communication (PLC), free space optic (FSO), satellite and the broadband fixed wireless access network. These different technologies are described below.

DSL technologies are based on the twisted copper pair used to provide telephone service. By transmitting signals at higher frequency through telephone wires, these systems are able to proved broadband services to users limited by distance to the local exchange and cable quality; thereby they proved broadband services to users with limited capacity.

HFC is derived from the cable TV network and provides a two-way communication between the head end and the subscriber. It is a shared-medium technology that is primarily a residential access technology.

FTTH is the best solution among wire line based broadband solutions with respect to transmission rate with several GHz capacities. However, fibre is expensive to install.

PLC is an access technology where power lines are used for providing broadband services. PLC has a potential to function as an access network technology with limited capacity and coverage. The idea behind PLC is that most homes are connected to power lines therefore instead of digging to install fibre; PCL can be used as carriers of fibre optic to costumers.

FSO is a ‘laser through the air’ technology, which is often used to interconnect the local area networks (LAN) between buildings of the same company (or on campus between university buildings) the technology uses lasers for short range, high capacity communications. The main advantages of FSO are the high data rate capacity and the fact that electromagnetic (EM) spectrum at optical frequencies well above 350 GHz is unregulated. Free-space optics systems therefore can be set up very rapidly without the need for any licenses or regulatory approval. Because high loss at these high frequencies, FSO links require that very careful alignment be maintained between the transmitter and the receiver.

Satellite communication systems are also used to deliver broadband services; usually the system is digital video broadcasting with return channel via satellite (DVB-RCS), it is often used in conjunction with wireless local loops for example WiFi or WiMAX. The downlink is divided in transport streams with 30 MHz wide and with QPSK modulation it has 36 Mbit/s capacities. The content in one transport capacity can be TV or data, and the data can be addressed individually or can be multicast.

BFWA is wireless broadband communication system that provides reliable digital two-way voice, video/audio and Internet services (triple play) to fixed users, and nomadic users. Fixed broadband networks use radio connections at frequencies above 20 GHz, in a point-to-multipoint (PTM) or ad-hoc configuration to send and receive traffic in a manner similar to wire line networks. These networks differ from mobile wireless by the fact that the endpoints in fixed wireless solutions are stationary and therefore less susceptible to the bandwidth and quality limitations associated with mobile wireless networks.

BFWA networks have several advantages over these alternative solutions. First, there are many places that do not have access to the last-mile wire line access technologies discussed above. These include rural areas with low population density, remote geographical areas, and urban areas with aged communication infrastructure. Many third world countries lack the basic telecommunication infrastructure required to support advanced communications systems. This lack of basic infrastructure, which is sometimes coupled with inhospitable terrain, makes conventional solutions prohibitively expensive and slow to deploy. Such places are good candidates for the fixed wireless broadband access solution, which can be deployed more rapid than any other technology. There is a window of opportunity for using BFWA as DSL coverage decreases due to high transmission rates and thereby short range. Figure 1 summarizes most of the existing broadband access technologies.

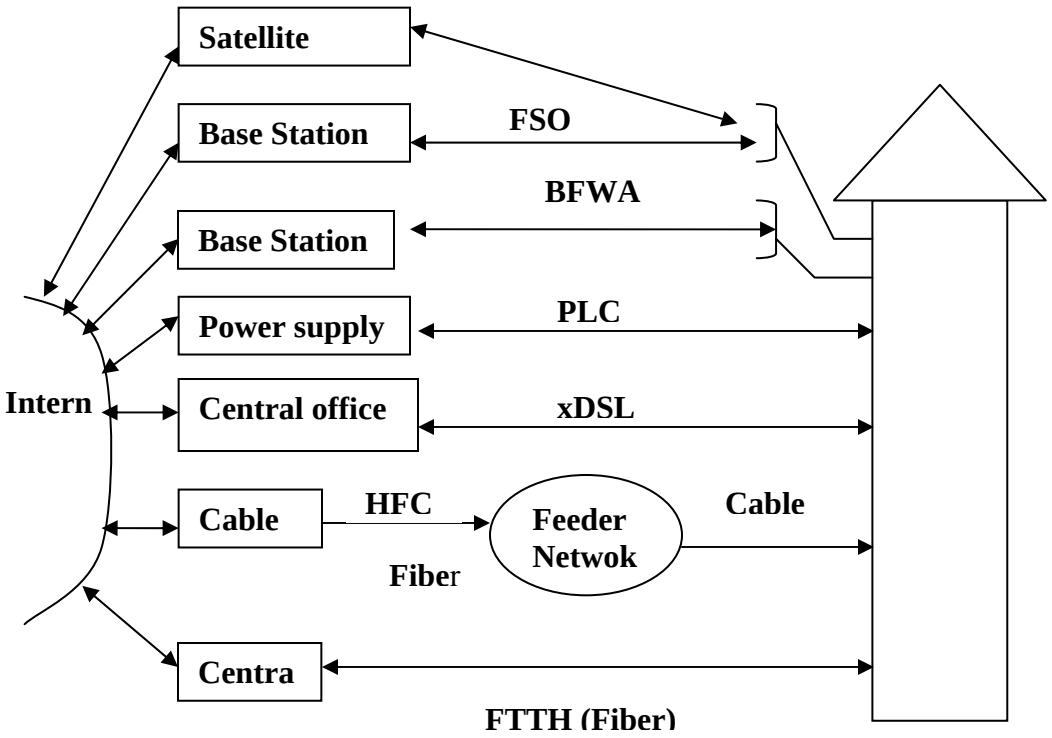

Figure 1. Different last-mile access technologies

2.1 Broadband fixed wireless access

As previously mentioned BFWA is wireless microwave broadband communication system that provides broadband services to end-users, and other base stations, such as wireless local area network (WLAN). The IEEE 802.16, Air Interface for Fixed Broadband Wireless Access Systems [6], is a standard for BFWA and specifies the air interface, including the medium access control layer (MAC) and physical layer (PHY).
The standard deals with two different frequency bands:

- Bellow 11 GHz
- 10 - 66 GHz

The European telecommunications standards institute (ETSI) and its committee for broadband radio access network (BRAN) has worked on several standards for wireless networking, one of them is ETSI HIPERMAN which is design for interoperable fixed broadband wireless access in the 2 – 11 GHz frequency range, with the air interface designed primarily for PMP.

WiMAX, which is an industry-led, non-profit corporation, formed to promote and certify compatibility and interoperability of broadband wireless products, which comply with IEEE 802.16 and ETSI HIPERMAN wireless MAN standards.

There are three main different architectures for BFWA; these are point-to-multipoint, point-to-point and mesh networks. These configurations are discussed in the sections to follow.

2.1.1 Point-to-multipoint (PTM)

This configuration is like a cellular concept where there is one base station (BS), and several customer premise equipment (CPE) communicating with the base station simultaneously, this is the most commonly used architecture. Figure 2 shows an example of point-to-multipoint architecture.

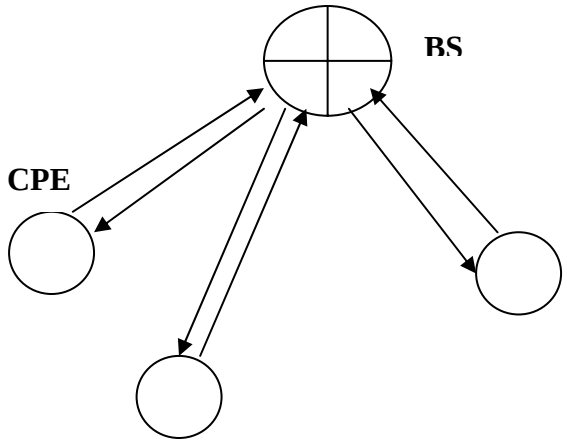

Figure 2. Point-to-multipoint architecture, where one BS communication with several CPE's

2.1.2 Point-to-point (PTP)

This configuration is a PTP connection between a base station and customer premise equipment, or a link between two base stations. Usually PTP configurations are used to transfer data between to base stations or backbone connection with the network. They usually use highly directional transmitting and receiving antennas. Figure 3 demonstrates the PTP architecture.

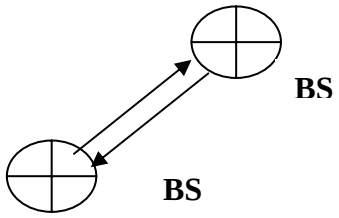

Figure 3. PTP connection between to base stations

2.1.3 Mesh network

This is a special BFWA architecture, which may give a line of sight (LOS) situation in an environment where there is not direct line of sight to the base station, roughly around obstacles. In the mesh concept every node (CPE) is able to route traffic to other nodes (CPE). Thus once a node is able to connect to any other node in the network, it automatically has access also to all the others. This enables better coverage with less power required and additionally in most cases, forms redundancy through availability of several routes. Also neighbours will be selected more on a LOS (if available at all) weight than on the location thus ensuring that rain attenuation from convictive heavy rain cells are rather avoided by using routes around them than by using excessive power to punch through. In other words in mesh configuration, there is always a line of sight to the base station, and in the case of bottleneck traffic in a given link, the system has an opportunity to reroute traffic to anther rout through different CPE. The disadvantages are, expensive and complicated CPE's having omni-directional antenna which can collect more interference than directional antenna, and since traffic is rerouted through different CPE's, the logging on and off of users can lead to loss of data, while the signal is in transit from source to destination. Figure 4 shows the mesh architecture.

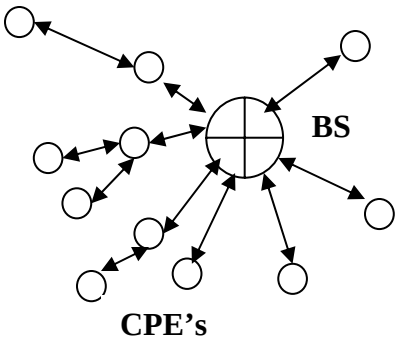

Figure 4. Mesh network

3 Radio wave propagation in BFWA systems

Maxwell's equations are used to predict the existence of propagation electromagnetic waves [7]. These equations specify the relationships between the variation of the vector electric field *E* and the vector magnetic field *H* in time and space within a medium. EM waves are also referred to as radio waves or radio signals. By solving Maxwell's equations one can predict radio signals. Among other factors this requires a perfect description of the complex environment (which is not available) in which the radio wave propagates. The equations are highly complex so that an extreme amount of processing power is necessary to solve the equations even for simple cases. Simpler models are thus developed for practical radio signal predictions in today's wireless communication systems. This section describes some of the theories this thesis is based up on; some basic propagation mechanisms, and channel characteristics are presented in the sections to fellow.

3.1 Propagation mechanisms

A propagation channel is a media where signals propagate to reach to their destination. In BFWA signals propagate through air, and when radio waves propagate from transmitter to the receiver the signals reach the receiver through the process of reflection, diffraction, refraction, scattering from buildings, structures, vegetation, rain and other obstructions in the path, and this can results in multipath propagation, where a multiple copy of the transmitted signal is received at the receiver with different phase, amplitude and delay. In addition signals undergo degradation and depolarisation due to rain in the propagation channel. Signals are also affects by dynamic vegetation effects, scintillation effects and other atmospheric effects (atmospheric absorption especially from water vapour (H_2O) and oxygen (O_2)). Figure 5 shows an example of multipath propagation.

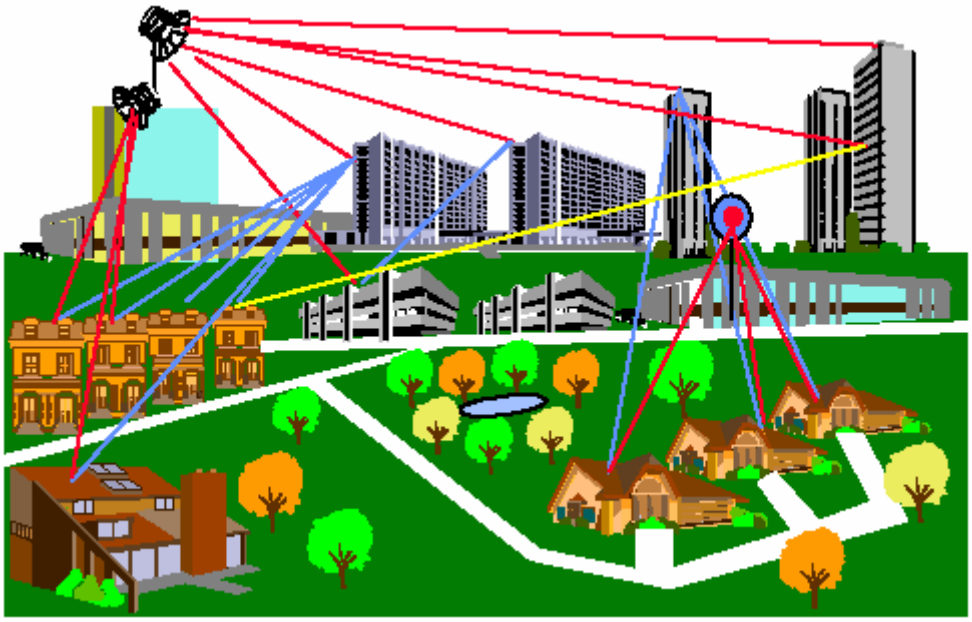

Figure 5. Illustration of multipath propagation in BFWA

Figure 5 shows typical multipath propagation where the receiver receives different copies of the same signal each having different amplitude, phase, and delay. Multipath will cause amplitude, phase fluctuations, and time delay in the received signals. These different signals received at the receiver can be out of phase, and can cause a reduction of the received signal strength, called multipath fading.

The impulses corresponding to the multiple paths arrive at the receiver at different times and with different amounts of power depending on the nature of the propagation environment that is responsible for the generation of the particular component. These multiple arrival times of signals with different powers can be used to define the impulse response of the channel, which is defined as the response of the channel to a transmitted signal. For example, in rural area these impulses are likely to arrive at almost the same time. This is due to the fact that there are fewer tall structures, and therefore the paths are close to each other. This means that the difference between arrival times of any information received will be too small to be observable or measurable such a channel is called flat fading channel, which means that the signals frequency are equally affected. On the other hand, for an urban area, the multiple paths will be more diverse and the received pulses will be spread out much more [8]. Under these conditions, information arriving in the form of finite pulses will overlap and result in broadened pulses, as shown in the Figure 6. Such a channel is called frequency selective channel, and the channel does not equally affect the signals frequency. Figure 6 shows the effect of frequency selective channel.

a) Transmitted pulse b) Received overlapped pulses

Figure 6. Frequency selective channel (a) A transmitted pulse. (b) The multiple pulses produced due to the multipath arriving at different times and with different powers, leading to a broadened envelope of the pulse.

3.2 Delay characteristics

Time dispersion of the channel is caused by multipath components arriving at the receiver with different excess delays, and plays a major role in the design of equalizer for high-speed wireless modems. It is stated in [9] that the time dispersive nature of the propagation channel can be characterized using parameters such as average excess delay and rms delay spread which are evaluated from the power delay profile (PDP). These are useful in the choice of suitable data rates and codec to avoid inter-symbol interference, which occurs when symbol period is greater than the delay spread. For BFWA operating above 20 GHz with high data rates this time dispersion can lead to inter-symbol interference in the system. The power delay profile is given by:

$$\hat{p}(\hat{\tau}) = \frac{E\left[\mathrm{h}(\mathrm{t},\tau)\right]^2}{2} \tag{1}$$

where $h(t,\tau)$ is the channel impulse response. Figure 7 shows an example of power delay profile with its different parameters.

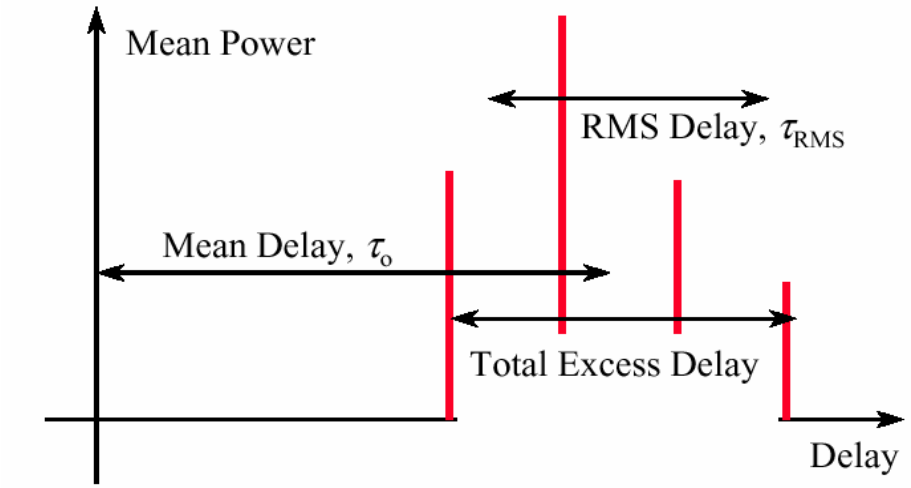

Figure 7. Power delay profile, taken from [9], page 241

The power delay profile parameters are:

- Excess delay, which is the delay of any tap relative to the first arriving tap
- Total excess delay, which is the difference between the delay of the first and last arriving tap; this is the amount by which the duration of a transmitted symbol is extended by the channel.
- Average (mean) delay τ_0, which is the power weighted average of the excess delays given by the first moment of the impulse response. (The delay corresponding to the centre of gravity of the profile); and it is defined by:

$$\tau_0 = \frac{\sum_{n=0}^{L-1} \tau_n p(\tau_n)}{p_m} \tag{2}$$

where, L is the total number of paths and p_m is the total energy given by:

$$p_m = \sum_{n=0}^{L-1} p(\tau_n) \tag{3}$$

- Rms delay spread τ_{rms}, which is the power weighted standard deviation of the excess delays given by the second moment of the impulse response and provides a measure of the variability of average (mean) delay, and it is defined by:

$$\tau_{rms} = \sqrt{\frac{\sum_{n=0}^{L-1} (\tau_n - \tau_0)^2 \, p(\tau_n)}{p_m}} \tag{4}$$

where $p(\tau_n)$ is the power delay profile and τ_n is the excess delay. Reference [10] states that, the correlation bandwidth is inversely proportional to τ_{rms} and can be used to study the wideband channel behaviour in frequency domain. For reliable communication without using adaptive equalization or other anti-multipath techniques, the transmitted data rate should be much smaller than the inverse of the rms delay spread which is called the coherence bandwidth. When the transmitted data rate is much smaller than the coherent bandwidth, the wireless channel is referred to as the flat channel or narrowband channel (fading affects all frequencies in the signal equally). When the transmitted data bandwidth is equal to or larger than the coherent bandwidth, the channel is called frequency selective channel or wideband channel (the depth of a fade for any given multipath condition at a given point in time will be different at different frequencies).

3.3 Time dynamic channel characteristics

The transmission characteristics are not determined by attenuation alone, and are not constant for any distance and time. The signal received may also fluctuate with distance and time, and the time varying fluctuation of the signal is caused by the random nature of the propagating environment such a channel is called time varying channel. In BFWA time variability arises as a result of movement of scatters and reflectors near the propagation path as a result of wind or movement of vehicles, vegetation, meteorological particles such as raindrops, etc. To deal with a time variant channel, Bello [11] defined the input delay spread function $h(t, \tau)$. This is the response of the channel at some time t to a unit impulse function input at some previous time τ seconds earlier. The time varying impulse response is defined as:

$$h(t,\tau) = \sum_{n=1}^{N-1} m(t_n, \tau_n)\delta(t-\tau)e^{-j(w_c\tau_c+\varphi)} \tag{5}$$

Where n is the tap index, N is the maximum number of taps, ω_c is the carrier angular frequency, τ_n is the excess delay of each multipath component, and ϕ is the random phase in the range $[0, 2\pi]$. The total received signal $y(t)$ is obtained by convoluting the channel impulse response with the transmitted signal $x(t)$ and adding additive white Gaussian noise, $n(t)$;

$$y(t) = x(t) \otimes h(t,\tau) + n(t) \tag{6}$$

Figure 8 shows the relationship between input/output signal, propagation channel, and noise.

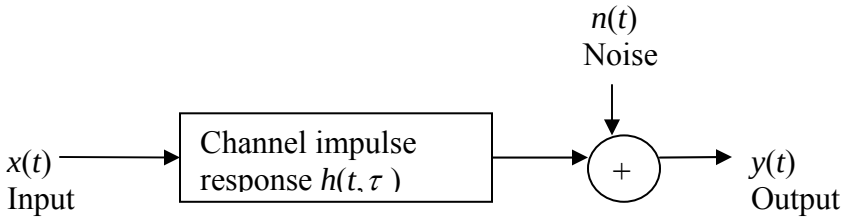

Figure 8. Received signal as a function of, transmitted signal $x(t)$, the channel response $h(t, \tau)$ and additive white Gaussian noise $n(t)$

The dynamic behaviour of the propagating channel can be studied though first order and second order statistics. The probability density function (PDP), which describes the probability of signal envelope, and cumulative density function (CDF), which gives the percent of time signal lies below a given level, or complementary cumulative density function (CCDF) which gives the probability that signal level lies above a particular level are first order statistics which can only be used to obtain static metrics associated with the channel, such as the bit error rate (BER) [12].

The second order statistics are level crossing rate (LCR) and average fade duration (AFD). LCR is a quantitative description of the rate at which fades of any depth occur. The LCR at any specified level is defined as the expected rate at which the envelope crosses that level in a positive-going or negative going direction.

AFD measures the average time interval the signal is below the threshold. Fade duration statistics provide information on outage period, or system unavailability due to propagation impairments on a given link and service. Understanding this scenario is important in dealing with burst of errors caused by fading, and by appropriately choosing interleaver length we can prevent burst of errors at the demodulator, in other words average fade duration is a key element in the process of choosing forward error correction code and best modulation schemes. Other important second order statistic is interfade duration, which is defined as the time interval between two crossings below the same attenuation threshold, and fade slope, which is defined as the rate of change of attenuation with time. The above mentioned second order statistics represent the dynamic representation of the channel. Both first order and second order statistical characteristics provide valuable information on the coverage limitations, choice of suitable data rates, word lengths and modulation and coding schemes in an operational BFWA system.

3.4 Channel models

In order to predicate and study the performance of BFWA system in terms of capacity, coverage and interference, we need to have a channel model that best descries the propagation channel. Propagation models are fundamental tools for designing any BFWA communication system. A propagation model basically describes what will happen to the transmitted signal while in transit to the receiver. In general, the signal is weakened and distorted in particular ways and the receiver must be able to accommodate the changes, if the transmitted information is to be successfully delivered to the recipient. Therefore choosing and applying the appropriate propagation model is an important aspect of wireless system design. As it is stated in [13], channel models will be divided into two basic classifications; these are empirical models and physical models.

3.4.1 Empirical models

Empirical models are based on measurement or observations of signal, in real propagation environments. To create such a model, an extensive set of measurements is made, and an appropriate function is fitted to the measurements, with parameters derived from the particular environment, frequency and antenna heights so as to minimise the error between the model and measurements [13]. The model can then be used to design systems operated in similar environments to the original measurements. The inability to explicitly account for particular features of the propagation environment is perhaps the greatest limitation of empirical, measurement-based models. The accuracy and usefulness of such empirical models also depend on the environment in which the original data for the model were taken and how universally applicable that environment is. A common problem is trying to use empirical models in areas where the propagation environment is widely different from the environment in which the data were gathered.

3.4.2 Physical models

Physical models make use of the physical mechanisms of electromagnetic wave propagation, same times called deterministic models. One aspect that affects the capabilities and success of a physical model is the kind of information about the propagation environment it can use and what it does with it. This is an important point about physical propagation modelling. The quality of the model's prediction is a direct consequence of how the model maps the real propagation environment into the model propagation environment [13]. It is also possible to combine both physical and empirical modes to account for both physical characteristics of the environment and measurements taken in that environment, these models are called physical-statistical models.

3.4.3 Tapped delay line channel model

BFWA systems operating above 20 GHz have large available frequency spectrum, and if the operating signal bandwidth is greater than the coherent bandwidth of the channel, it becomes a dispersive frequency selective channel. Such a wideband channel is generally characterised by tapped delay line model. Tapped delay line channel model is represented by time-variant finite impulse response (FIR) filter in complex equivalent low-pass signal domain. Figure 9 shows a tapped delay line channel model representation.

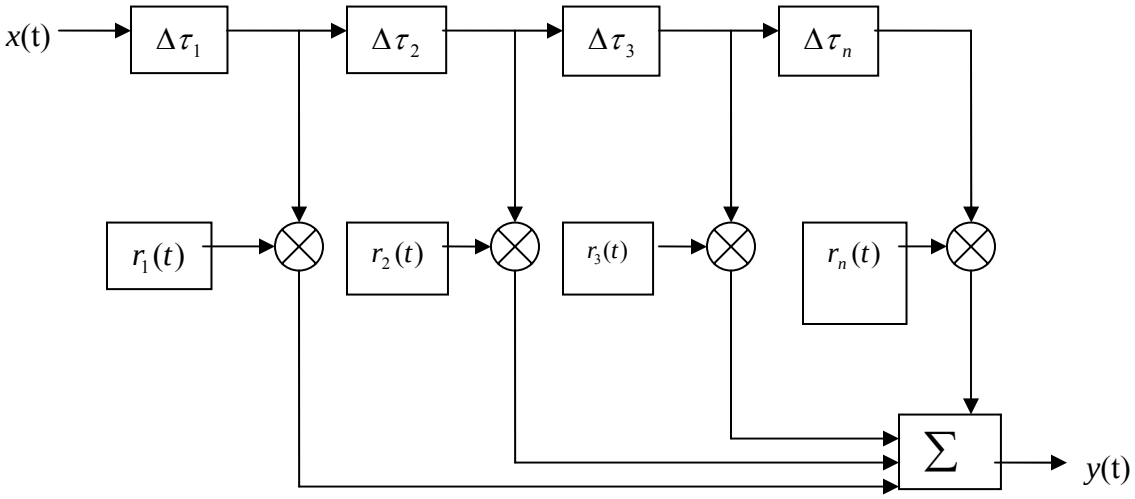

Figure 9. Tapped delay line model for channel response. $x(t)$ is the input signal, $\Delta\tau$ is the delay, $r_n(t)$ is a time varying gain, and $y(t)$ is the output signal

In this model the output signal is the sum of the input signal time delayed by $n \cdot \tau$ and multiplied by a time varying tap weight function. The choice of delay times $\Delta\tau$ is somewhat arbitrary (random) but is usually related to the symbol and the channel characteristics. In Figure 9 the delay times are shown as being equal but this is not strictly necessary.

The significant features of this model are the multiplicative functions $r(t)$. Each of the delay taps essentially creates a time bin. All of the waves arriving during the time bin are vectorally added together to create the function $r(t)$, and those waves can be in or out of phase with each other leading the envelope of $r(t)$ to vary. The result is that $r(t)$ describes as time varying amplitude and phase of the reflected signal.

Generally, a PDP represents the variation of relative power density of the signal received as a function of average time delay. The most common decay function is an exponential decay function. For example, for some mobile systems the PDP is represented by two exponential decay functions, one represents taps from local scatters and the other from remote scatters. Since most BFWA systems operate in line of sight (LOS) configuration, most of the scatters are buildings or objects in the vicinity of the receiver (local scatters). Therefore the PDP of BFWA is mostly represented by one exponential function. A

number of parameters have to be specified when developing a tapped delay line channel model, these are:

- Number of tapes N
- Excess delays of the taps τ_n
- Relative (average) amplitudes of the taps $\alpha_n = r(t)$
- Amplitude distributions of the taps $p(e,\phi)$ as function of envelope and phase
- Correlation between consecutive taps

The minimum number of taps N can be evaluated using the following simple relation [14],

$$N = \tau_{\max} * B \ + 1 \tag{7}$$

where $\tau_{\max}$ is the maximum tap delay and B is the signal bandwidth. As mentioned above the delay of taps can be arbitrary, but usually chosen to be related to the symbol duration time of the symbols transmitted in the channel, for example 8 -16 times the symbol rate. The average amplitude of each tap has to be specified, this can be obtained from measurements. Because of the time dynamic nature of the channel, the amplitude of each tap also varies with time. The most common used distributions for the tap envelopes are:

- Rayleigh distribution
- Nakagami-Rice distribution
- Nakagami-m distribution

Depending on the propagation characteristics the average tap amplitude varies according to one of the above distributions. In order to model the channel variation, knowledge of Doppler spectra of each tap is required, and then by taking the inverse Fourier transform, the autocorrelation function of each tap is determined. Since the received signal is the convolution sum of all taps, in order to know the received signal variation over time, the knowledge of correlation between each tape is required. Generally the sources in the propagation environment that cause the multipath wave can be classified as scatters. The common assumption is that these fading functions are uncorrelated, giving rise to the tapped channel model being described as wide sense stationary uncorrelated scattering (WSSUS). This means the taps are uncorrelated, and the correlation value depends only on the difference in time lag between taps, not the time of occurrence of each event.

4 System description

This section describes the communication system for which the dynamic channel model is developed. The system is a PTM system, operating between 20 – 50 GHz; in our study we specially focus at 40 GHz. The system uses time division duplex (TDD), where the same frequency is used for both downlink and uplink transmission separated by time. The signal bandwidths under consideration are 112, 56, and 28 MHz. The system uses single carrier with Nyquist filter and N – QAM modulation, where N = 2, 4, 16, 64.

4.1 System performance

The CPE in BFWA system typically has a narrow beam antenna pointing directly at the base station. The base station antenna may have a wider antenna beam width typically 90 – 120 degrees. Base station antennas considered in this study have opening angles of 90^0, 60^0, and 40^0 respectively. Since antenna beam width plays an important roll in limiting the amount of multipath and interference received, the channel model should include antenna beam width as model parameter.

Since the system uses TDD, in addition to base station to CPE interference, there is BS-to-BS interference, which can dramatically reduce the system capacity. BS-to-BS interference can be eliminated in a TDD system by aligning the uplink and downlink intervals for all the BS's in an area. But this approach reduces the main advantage of TDD in adapting the traffic between uplink and downlink and requires an accurate synchronization of the base stations that leads to extra system complexity.

On the other hand, if the TDD uplink/downlink bandwidth allocation is set independently in all sectors, harmful interference situation will arise. Both user terminal in uplink mode and sectors in downlink mode can cause interference in to sector in uplink mode. Co-channel interference from a sector in downlink mode to a sector in uplink mode has a very high probability of occurring.

There are a number of interference mitigation techniques, such as interference cancellation between two base stations, smart antennas, and adaptive coding and modulation, etc. In order for these mitigation techniques to work properly and effectively, there is a need for having time dynamic channel model, which properly describes the propagation channel. Figure 10 shows how interference cancellation technique depends on the knowledge of propagation channel.

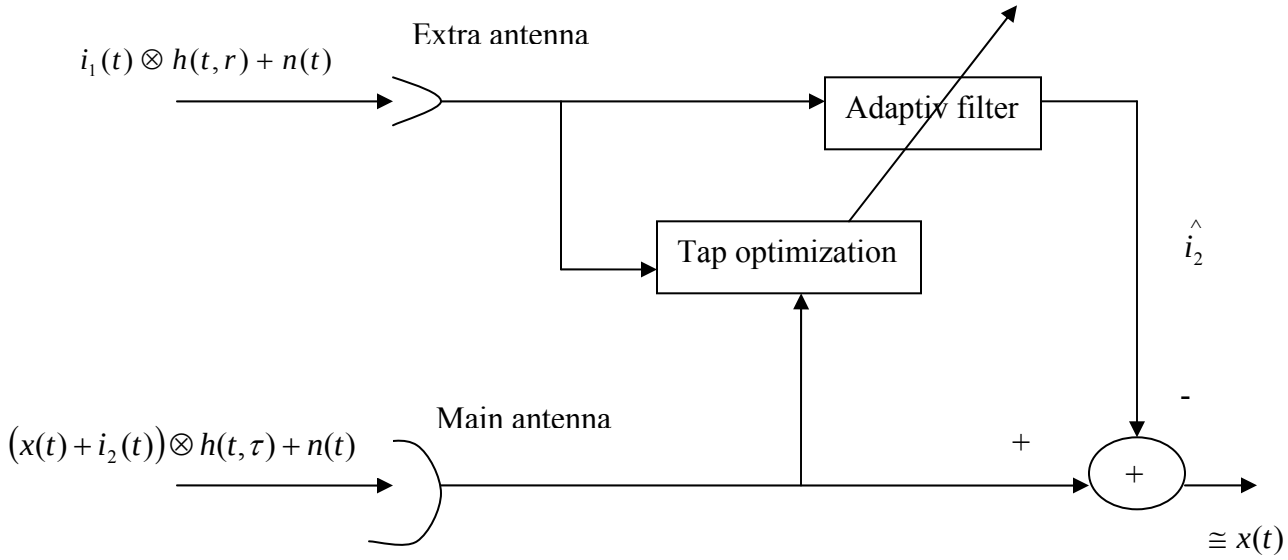

Figure 10. Main principles of inter base station interference cancellation

The transmitted signal $x(t)$ and the interfering signal i_2 are summed and convolved with channel impulse response $h(t,\tau)$, and are received by the main antenna at the base station. In addition the base station has an extra directive antenna which points to words the interfering base station, so that the amount of interference signal received by the main antenna can be estimated from the extra directive antenna thereby cancelling the interference. Since we estimate i_2 form i_1 and channel impulse response $h(t,\tau)$, we need to have a dynamic channel model that characterizes the channel impulse response $h(t,\tau)$ properly in order to increase the ability of mitigation techniques.

5 Measurements and channel models for BFWA systems

In this section we discuss reported wideband and narrowband measurements made at different places in the word in frequency range between 20 to 50 GHz. These measurements were conducted in order to characterise the wideband frequency selective effects (multi-path) and narrowband flat fading effects (rain and vegetation) of BFWA systems operating above 20 GHz. In addition existing wideband channel models and dynamic models of rain and vegetation are discussed.

5.1 Wideband multipath measurements and models

BFWA systems operating above 20 GHz have large available wide bandwidths, in addition at this frequency rang wideband signals are susceptible to frequency selective fading due to multipath propagation. In this section the wideband multipath measurements and existing tapped delay line models (static and dynamic) for BFWA systems are discussed. In addition, the dependency of channel multipath property on rain, antenna height and directivity is discussed, followed by discussions on the statistical description of the wideband channel.

5.1.1 Tapped delay line channel models for BFWA systems

P. B. Papazian, G. A. Hufford, and R. J. Achatz [15] reported measurements made in Northglenn, Colorado and in San Jose, California to study area coverage, multipath, and depolarization for two suburban neighbourhoods, were the most important difference between sites are vegetations, in particular the tree canopies. The measurements were made at 28.8 GHz narrowband continuous wave signal and at 30.3 GHz for a wideband signal. The narrowband data was used to study area coverage, short term time variations of the signal, depolarization and cell-to-cell coverage, while the wideband date was used to study multipath properties. These signals were received using a parabolic dish antenna, and then split, down converted and processed in separate receivers. They used a vertically polarized horn transmit antenna with 14 dBi gain, and 3 dB beam width of 90^0, 20^0 in azimuth and elevation respectively. The receiver antenna system consisted of two 2.5^0 dishes with linearly polarized feeds. One dish was aligned for vertical polarization and the second was aligned for horizontal polarization.

In the development of the model they selected three stations located at successively greater distances from the transmitter along the same cell radial to represent good, moderate, and bad wideband channels. From the wideband measurements they proposed a tapped delay line channel model that represents good, moderate, and bad wideband channel. Table 1 summarizes the channel model at these stations, and Table 2 lists the distance D between transmitter and receiver, attenuation A, delay spread S and L_b (free space loss plus attenuation).

Quality	Tap number	Tap gain, β_n (dBm)	Tap delay, τ_n (ns)
Good	1	0	0
Moderate	1	0	0
Moderate	2	-13.7	5.3
Bad	1	0	0
Bad	2	-2.8	3.6
Bad	3	-16.2	15.3

Table 1.Summary of tapped delay line models for good, moderate, and bad channel.

Quality	*D* (m)	*A* (dB)	*S* (ns)	L_b (dB)
Good	122	6.2	1.26	111.7
Moderate	309	32.2	1.60	145.9
Bad	419	32.6	2.95	159.4

Table 2. Summary of distance *D*, attenuation *A*, delay spread *S* and basic transmission loss L_b at 99 % exceed for three wideband channels in Northglenn, Colorado.

The small delay spreads confirm that there are few specular reflections due to the filtering effect of the narrow beam receiver antennas. From Table 2 we see that links, which exhibit multipath, also have larger values of transmission loss L_b and attenuation *A*. One explanation is that the multipath is caused by multiple scattering events.

P. Soma, L. Cheun, S. Sun and M.Y. W. Chia [1] conducted measurement in urban, suburban and rural environment in Singapore and developed static and dynamic wideband channel model for BFWA. In their measurement, a signal bandwidth of 200 MHz is transmitted through a vertically polarized omni-directional antenna with 11 dBi gain, fixed on the rooftop of a building located on a hill such that it can be seen by most of the receiver locations ranging from 500 m – 5 km. The receiver has a flat panel antenna with a gain of 31 dBi and a 3 dB beam-width of 4^0 in both the azimuth and elevation planes. The receiver sites were usually surrounded by several residential blocks, business centres, and foliaged sport grounds and by hilly terrain. The measurements were carried out on the rooftops of various 13 and 25 storied residential blocks located in urban, suburban, and rural areas. It was noticed from measurements that the longer delayed multipath clusters are 25 dB weak compared to the direct LOS signal. In the development of the model they made a number of assumptions, including:

- Line of sight condition exists between transmitter hub and receiver antennas, both mounted on rooftops.
- Complete blockage of receiver and heavy rain conditions were not considered
- Multipath components below -30dB compared to direct LOS signal were excluded.

The receiver sites were classified to have good, moderate and bad channel based on the environmental loss (which varies from 4 to 40 dB for various locations). The major contribution of the environmental loses was observed to be the local blockage conditions. It was observed that delay spread increases linearly with the environment loss, and a linear relationship was derived. The measured excess path loss and delay characteristics of static channel impulse response are summarised in Table 3 for various channel types.

Channel Type		Mean Delay (ns)	Delay Spread (ns)	Excess Loss (dB)
Good	Model 1	15.46	11.96	0-12
	Model 2	22.46	14.61	
	Model 3	31.72	18.16	
	Model 4	27.10	16.65	
Moderate	Model 1	28.97	16.67	12-26
	Model 2	35.27	50.89	
Bad	Model 1	18.87	13.69	26-40
	Model 2	85.35	75.84	

Table 3. Summary of the static channel models

The good channel impulse response (IR) models primarily represent locations having strong signal reception with environment loss in the range of 0 – 12 dB (typical rural area). It was also observed that the longer delayed multipath components are very weak compared to the direct LOS component. Static channel IR for good and moderate multipath are listed in Table 4 and 5 respectively. In these tables, the tap gain values were obtained by taking the average of all the IR measurements in the same channel type.

Excess Delay (ns)	Tap gain (model 1)		Tap gain (model 2)	
	Numeric	dB	Numeric	dB
0	0.74	-2	0.48	-6.31
20	1	0	1	0
40	0.4	-8.05	0.66	-3.67

Table 4. Good reception with fewer multipaths

Excess Delay (ns)	Tap gain (model 3)		Tap gain (model 4)	
	Numeric	dB	Numeric	dB
0	0.12	-18.18	0.29	-10.86
20	0.92	-0.69	1	0
40	1	0	0.79	-2.00
60	0.21	-13.45	0.08	-21.86
80	0.06	-24.54	0.10	-19.68
100	0.10	-20.00	0.09	-20.79

Table 5. Good reception with moderate multipath

Table 4 and 5 shows a channel model for good and moderate signal reception respectively; one can derive a single good channel IR model by taking the average of all four IR models assuming that the multipath components below –20 dB are insignificant. The environment loss is less than 12 dB for this group as listed in Table 3. The average power delay profile for these models is shown in Figure 11.

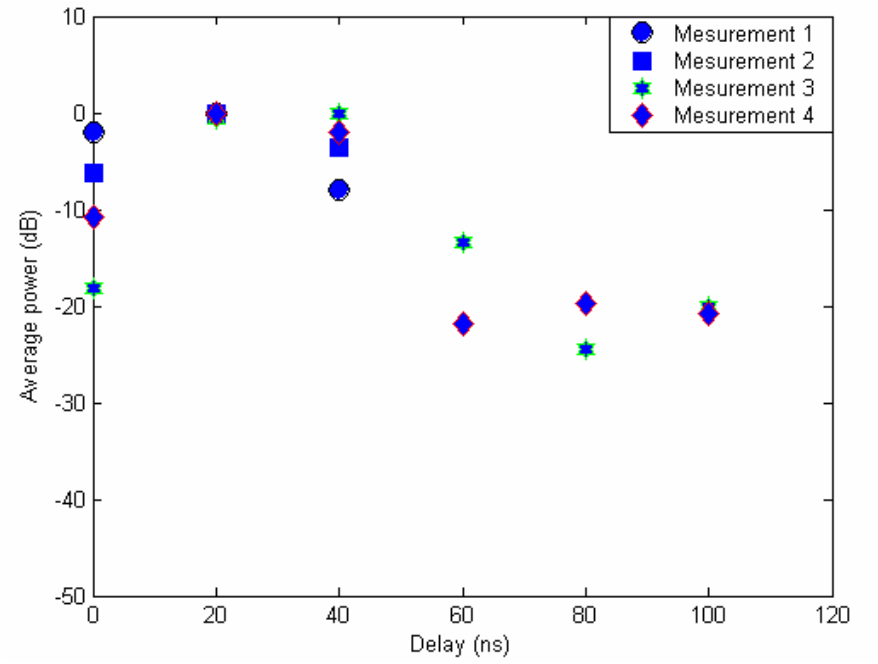

Figure 11. Measurement results form rural areas [1]

The moderate channel models represent locations with moderate signal reception having environment loss in the range of 12 – 26 dB and delay spread in the range of 20 – 50 ns (typical suburban areas). Tow types of IR were observed from measurements and are listed in Table 6. The signal to noise ratio (SNR) was observed to be 25 dB for these channel types.

Excess Delay (ns)	Tap gain (model 1)		Tap gain (model 2)	
	Numeric	dB	Numeric	dB
0	0.24	-12.36	0.48	-6.37
20	1	0	1	0
40	0.94	-0.50	0.58	-4.70
60	0.17	-15.56	0.12	-18.16
80			0.10	-20.00
200			0.10	-19.91
280			0.12	-18.71
300			0.15	-16.74
340			0.12	-18.68
360			0.13	-17.65

Table 6. Channel IR models for moderate signal reception

Figure 12 shows the plot of measurement 1 and 2 for comparing the models presented in Table 6.

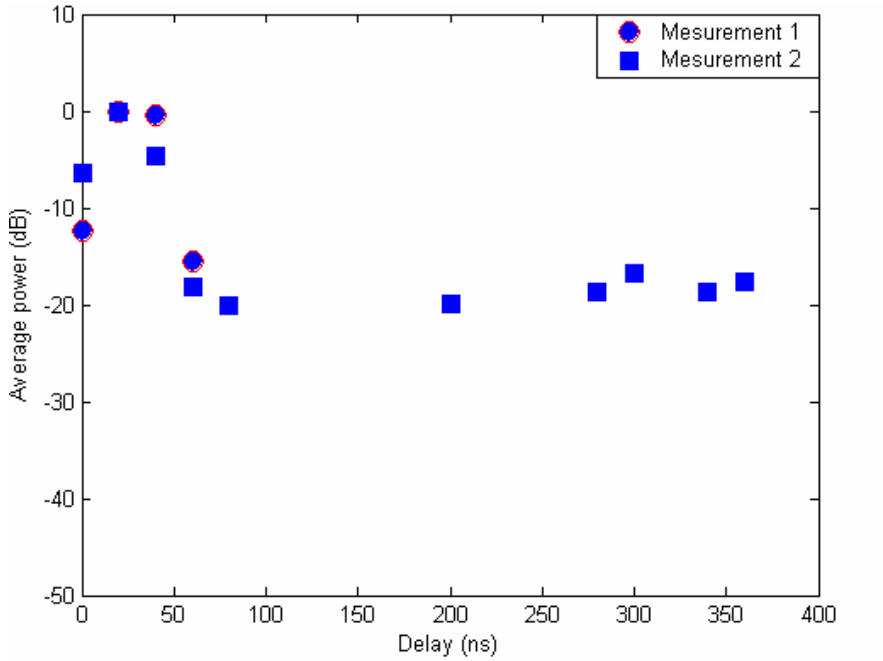

Figure 12. Measurement results form suburban areas [1]

The locations having heavy blockage conditions with environment loss varying from 26-40 dB were grouped into the bad channel type (typical urban areas). The two channel IR models observed form measurements are listed in Table 7.

Excess Delay (ns)	Tap gain (model 1)		Tap gain (model 2)	
	Numeric	dB	Numeric	dB
0	0.70	-3.05	0.70	-3.12
20	1.0	0.0	1.00	0
40	0.62	-4.10	0.52	-5.68
60			0.24	-12.31
80			0.35	-9.24
100			0.37	-8.64
120			0.24	-12.34
140			0.21	-13.43
200			0.23	-12.7
220			0.20	-14.1
260			0.27	-11.32
280			0.43	-7.27
300			0.42	-7.44
320			0.27	-11.3

Table 7. Channel models for poor signal reception

The channel model 1 listed in Table 7 represents the LOS location at large distances (5 km) during a rainy day, where the receiver SNR is only 8 dB. It indicates that when the main signal peak itself is weak due to the longer separation distance or rainy climate, multipath components are very significant. Channel IR model 2 in Table 7 corresponds to closer locations at a distance of 1.5 km from the transmitter. In these measurements, the SNR value is 15 dB. The higher delay spread values are due to the significant multipath components. Moreover, excess loss as high as 35 dB and maximum excess delay of 1240 ns are observed in this group. Figure 13 shows the plot of measurement 1 and 2 for comparing the models presented in Table 7.

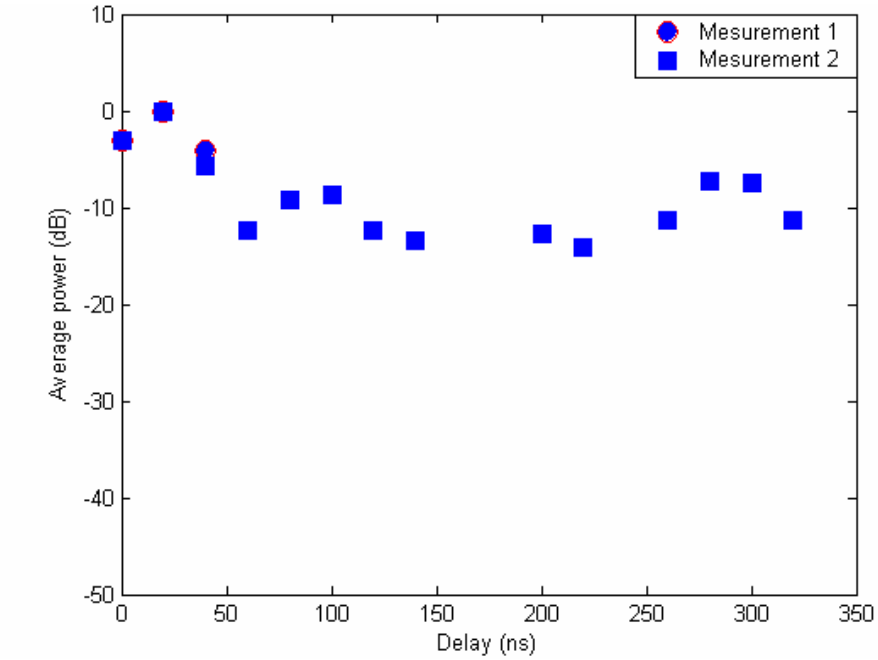

Figure 13. Measurement results form urban areas [1]

In addition to the static channel model, a time varying tapped delay line channel model for BFWA systems operating in urban, suburban, and rural areas was also reported in [1]. They define the time varying channel impulse response as follows:

$$h(t_k,\tau) = c_k \sum_{n=1}^{N-1} m(t_k,\tau_n)\delta(\tau-\tau_n)e^{-j(w_c\tau_c+\varphi)} \tag{8}$$

where n is the tap index of various multipath components, N is the maximum number of taps, w_c is the carrier angular frequency, τ_n is the excess delay of each multipath component, and ϕ is a random phase in the range [0, 2π]. The factor c_k is a random variable that models the time-varying nature of the peak of the impulse response. The peak signal level variations were observed to follow Nakagami-Rice distribution with K factors ranging from -4 to 12 dB. The function $m(t_k,\tau_n)$ represents the distribution of the tap gains of various multipath components of the channel impulse response. The two parameters c_k and $m(t_k,\tau_n)$ provide the distribution of the tap gains of various multipath

components at a given time and channel type. They used general equation to represent a particular multipath cluster at a given time:

$$m(\tau_n) = \alpha \exp\left\{-\beta\left(\frac{\tau_n - \tau_p}{100}\right)^2\right\} \tag{9}$$

Where β controls the rate of decay of tap gains, α is the peak amplitude, and τ_p is the peak time of a particular multipath cluster. The excess delay τ_n varies from 0 to a maximum delay of $\tau_{\max}$. Table 8 summarizes the channel impulse response parameters, and Table 9 classifies the time varying channel model.

Peak time, τ_p (ns)	Attenuation factor, α	Decay factor, β	Excess delay, τ
40	1.0	β_1	0 – 40
40	1.0	β_2	40 – 100
100	0.1	β_3	100 – 250
320	0.1	β_4	250 – 400

Table 8. Summary of time-variant impulse response model parameters

Parameter	Urban	Suburban	Rural
c_k (dB)	-10 – 6	-5 – 3	-5 – 3
β_1	20 – 100	50 – 120	50 – 120
β_2	6 – 20	10 – 25	10 – 25
β_3	0.5 – 10	1 – 10	0
β_4	5 – 50	0	0
$\tau_{\max}$ (ns)	400	250	100
Mean excess Delay (ns)	50 – 70	40 – 50	30 – 40
RMS delay spread (ns)	20 – 80	10 – 20	< 10
K- factor (dB)	-4 – 3	3 – 6	6 – 12

Table 9. Classification of time variant channel impulse response models

W. Zhang and N. Moayeri reported a tapped delay line model for BFWA systems, which includes no more than three taps [16]. The tap gains have a progressive decrease relationship, while the tap delays have a progressive increase one. The model is valid under the following assumptions: (1) there is LOS propagation, (2) highly directional antennas are used at least at the receiver, (3) heavy-rain attenuation effects are not taken into account, and (4) –20dB threshold is applied, which excluded multipath components with amplitudes below the threshold. The expression of the channel propagation model is

$$h(t) = \sum_{n=0}^{N-1\leq 2} a_n \delta(t-\tau_n)\exp(-j\omega_c\tau_n) \tag{10}$$

The channel impulse response $h(t)$ is normalized in the sense that $20\log_{10}a_0=0$ and $\tau_0=0$ ns for the ray that has the maximum amplitude. They recommend a decreasing order for the tap gain a_n as:

$$A_{\max} \geq 20\log_{10} a_1 \succ 20\log_{10} a_2 \geq A_{\max} \tag{11}$$

and an increasing order for the tap delay τ_n as :

$$\tau_{\min} \leq \tau_1 \leq \tau_2 \leq \tau_{mas} \tag{12}$$

Based on the wideband radio channel measurements [15], the values $A_{\max}$, $A_{\min}$, $\tau_{\min}$ and $\tau_{\max}$ are determined and listed in Table 10.

Items	$A_{\max}$ (dB)	$A_{\min}$ (dB)	$\tau_{\min}$ (ns)	$\tau_{\max}$ (ns)
Values	-2.8	-20	3	50

Table 10. Values of maximum and minimum for tap gain and delay

The value of $\tau_{\max}$ applies under the assumptions of LOS propagation and use of a highly directional receiver antenna. The value of $A_{\min}$ is set at a threshold of –20dB [15]. Available BFWA radio channel impulse response measurements support the model presented above. As evidence, measurements of [15] are presented in Table 1. It is seen that the good channel has one ray, the moderate channel has two rays, and the bad channel has three rays. On the basis of wideband measurements at 29.5 GHz, David Falconer [17] proposed a multipath model. This model is summarized in Table 11. Some measurements data were obtained at non-LOS sites. For the positive tap indices, equation (10) agrees with the model in Table 11 [17]. Physically, if tap index 0 indicates the direct ray, the taps having negative tap indexes disappear.

Tap index	$20\log_{10}a_0$ (dB)	τ_n (ns)
0	0	0
1	-15	20
2	-20	50
-1	-15	-20
-2	-20	-50

Table 11. Summary of a multipath model

Propagation in urban environment was specially studied by, C. Briso-Rodriguez M. A. Vazquez-Castro, and J. I. Alonso-Montes [18]. Channel measurements and modelling at 28 GHz, LMDS were conducted in order to classify propagation channel impairments according to parameterised urban environments. This is because in most reported channel models, environment is rarely parameterised in terms of geometric attributes such as building density and height. This leads to for example, report delay spreads for generic urban areas show significant disagreements from one measurement campaign to the other. In their studies they proposed a well-defined parameterisation of urban areas, namely as a function of statistical heights and width distributions. They note that within a given urban environment several, mean heights can be found depending on the district (city, historical centre, shopping area, etc), and they reflect in their studies where different districts were analysed in Madrid. Four different sectors of Madrid were investigated and heights were fond to be normally distributed, since these distributions describe heights, it should be more appropriate to designate them as truncated distributions (in order to avoid negative building height). Table 12 shows the parameters of heights distributions where μ is the mean, and σ the variance.

Location	General Description	Distribution
Zone 1	Business area, very high buildings	Normal μ=21.4 m, σ = 8.9 m
Zone 2	Residential area, old buildings with few stores	Normal μ=12.5 m, σ = 3.7 m
Zone 3	Historical and shopping centre of Madrid	Normal μ=10 m, σ=2 m
Zone 4	Residential area, new individual houses	h < 9 m 5 % h = 9 m 20 % h = 12 m 20 % h > 12 m 5 %

Table 12. Building Height Distributions [18]

The proposed environments (Zones) were measured using a time domain channel sounder. The transmitter antenna was a horn with 20 dBi gain, and a 3 dB beam width of 45^0 in azimuth and 6^0 in elevation. The receiver uses a more directive horn with a gain of 35 dBi and a 3 dB beam width of 3^0 in azimuth and elevation. With this system measurements were taken in different location of the four parameterised environments.

The transmitter was located in high buildings or towers and the receiver was moved in an area from 500 m to 5 km around it, and all the measurements were taken in line-of-sight. The measurements were processed to compute statistics of excess path loss, mean delay, RMS delay spread and correlation bandwidth for different urban classifications. Table 13 shows the results for the different environments measured. This result is important when urban propagation is considered, since a realistic urban definition is provided depending on the height and width distribution of buildings.

Location	**Zone 1**
Received power	-50 – 100 dBm
Mean delay	60 – 380 ns
Delay spread	50 – 200ns
Rice *K* factor	-3 – 12 dB
Excess path loss	10 – 60 dB

Location	**Zone 2**
Received power	-50 – 100 dBm
Mean delay	140 – 680 ns
Delay spread	150 – 300 ns
Rice *K* factor	-13 – 25 dB
Excess path loss	3 – 6 dB

Location	**Zone 3**
Received power	-50 – 100 dBm
Mean delay	40 – 150 ns
Delay spread	50 – 60 ns
Rice *K* factor	-8 – 15 dB
Excess path loss	8 – 12 dB

Location	**Zone 4**
Received power	-50 – 100 dBm
Mean delay	150 – 580 ns
Delay spread	100 – 150 ns
Rice *K* factor	-12 – 21 dB
Excess path loss	4 – 6 dB

Table 13. Parameters obtained for different locations (different urban types)

5.1.2 Multipath dependence on antenna height and directivity

Scott Y. Seidel and Hamilton W. Arnold [19] reported the dependency of multipath on receiving antenna height. The study was intended to evaluate the propagation characteristics of 28 GHz radio signals in a residential urban environment. Signal strength was measured at antenna heights over a range of 3.4 meters to 11.3 meters above ground level to determine subscriber antenna heights required to provide service. A pneumatic mast was used to hoist the antenna to heights of 4, 7.3 and 11.3 meters. The maximum height of 11.3 meters above ground level was higher than the two and three story buildings in the vicinity of the measurement at many of the locations. The middle height of 7.3 meters was often close to the rooftops of surrounding buildings, and the lowest height of 4 meters simulates a wall-mounted subscriber antenna.

Generally from the measurements they observe that the received signal level decreases when the antenna height was reduced from 11.3 to 7.3 to 4 meters, and at many receiver azimuth angles, the signal level received via reflection is greater at the lower antenna heights than when the mast was fully extended. At 11.3 meters above ground, the antenna was higher than the buildings in the immediate vicinity of the receiver and no reflections were observed from those directions. As the antenna was lowered, reflections from the buildings across the street were detected and the direct signal disappeared. Other important observation was in locations with line-of-sight to the transmitter, the received

signal level in the direction of the transmitter is unaffected by receiver antenna height. From this we observe that receiving antenna height affects the amount of multipath signal received.

CRABS [20] studied the effect of transmitting antenna beam width on the multipath property of the channel. It was observed that significant multipath effects would only occur if there were a large reflecting surface close to base station antenna that has a wide sector pattern in the horizontal plane. It was observed that the base station antenna beam width has implications for the amount of multipath propagation as well as on the angle of arrivals. The wider the base station antenna beam width is, the more potential scatters the base station sees, and the longer the propagation delay compared to the direct signal will be, therefore depending on the strength of the multipath component, the channel gets more frequency selective. Figure 14 shows the implications on multipath propagation when changing base station antenna beam width.

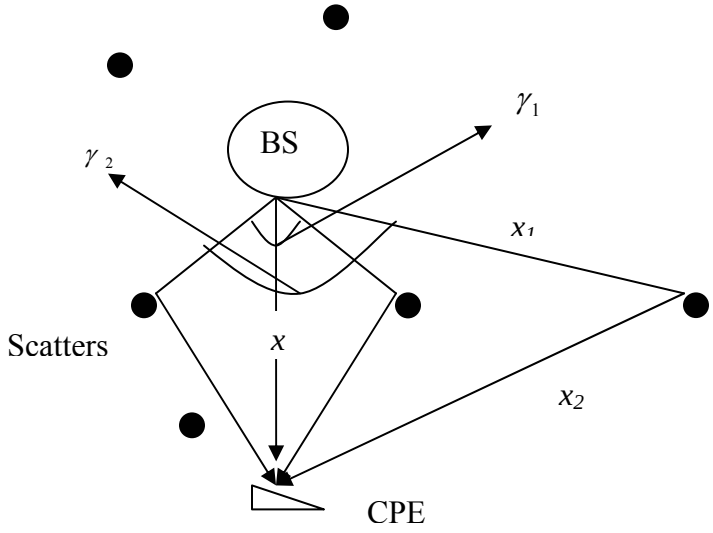

Figure 14. Antenna beam width and its impact on multipath

where x, x_1 and x_2 are different paths taken by the transmitted signal, γ_1 and γ_2 are two different base station antenna beam width. We observe from Figure 14 that the propagation delay increases as base station antenna beam width γ increases. The distance difference (Δd) between the direct signal x and the reflected signal ($x_1 + x_2$) is given by:

$$\Delta d = x1 + x2 - x \tag{13}$$

$$\tau = \frac{\Delta d}{c} \tag{14}$$

The time delay difference increase with increasing Δd, and Δd increases with increasing γ which is the base station antenna beam width. Due to the variations in antenna directivity, with a narrow beam user antenna and a wide beam base station antenna, channel models are required to properly weight the received multipath components

according to their angle-of-arrival. Assuming antenna radiation patterns according to ETSI EN 301 215-3, with base station sector angle of 90 degrees and the relatively wide beam user terminal antennas; we can calculate the worst-case potential multipath power (see Figure 15).

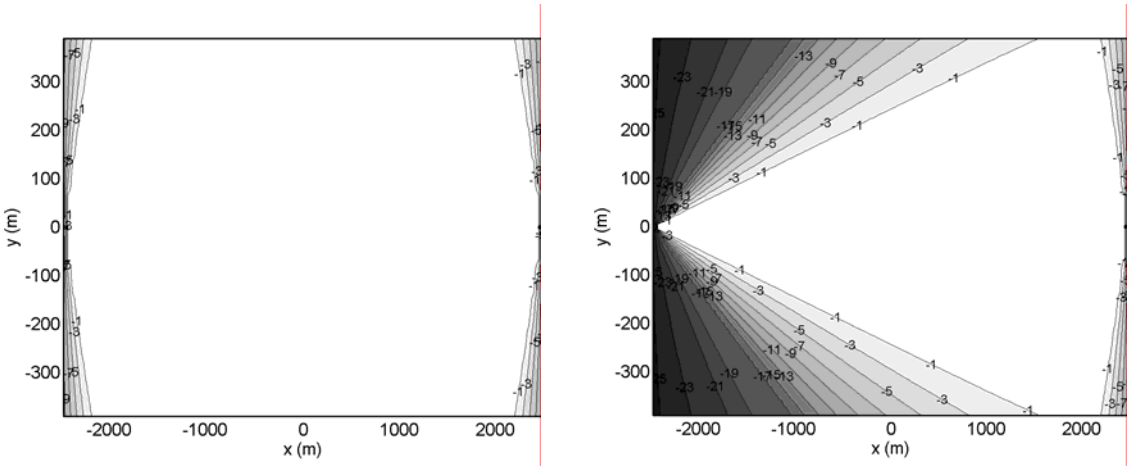

a) Base station to base station b) User terminal to base station

Figure 15. Multipath power contour dB plot

Based on the antenna diagrams, it is possible to draw relative power and time delay zone and then identify whether any reflecting surfaces are within these zones. Figure 16 shows an example of excess delay plot for two base stations located 5 km apart.

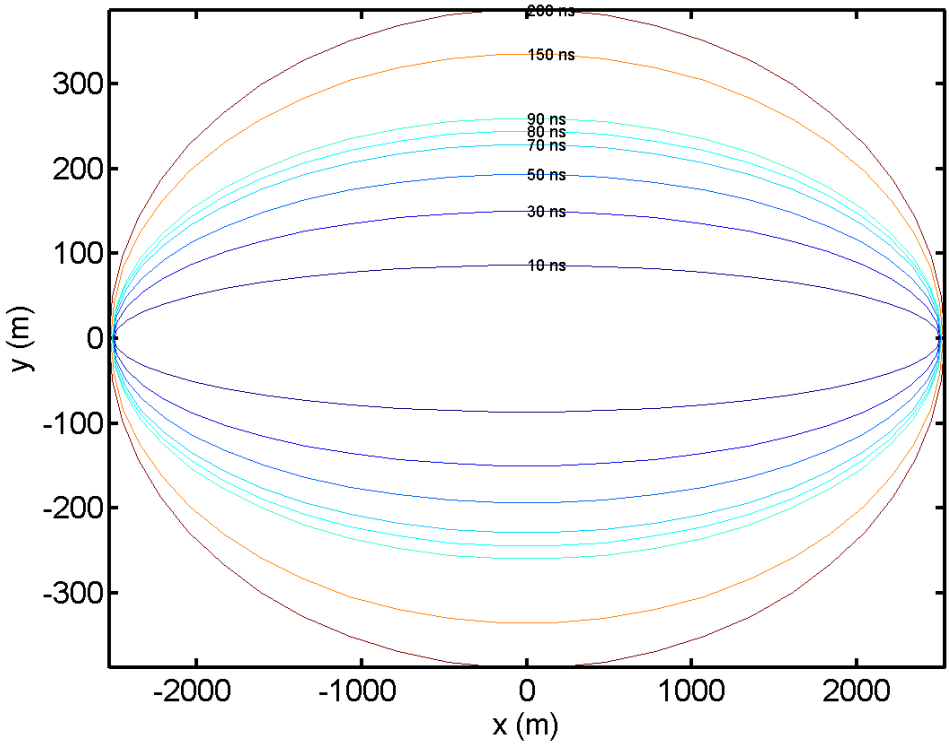

Figure 16. Excess delay contour plot, 5 km distance between two antennas

5.1.3 Multipath dependence on rain

Based on wideband measurement campaign at 38 GHz, the effect of various weather conditions on multipath was studied in [21]. The objective of the measurement was to determine multipath and time varying channel behaviour of short-hop millimeter-wave point-to-multipoint radio links during various weather events. In their measurement they used a sector horn vertically polarized transmitting antenna with 3 dB beam width of 45 and 6.5 degrees in both azimuth and elevation respectively, and 19 dBi antenna gain. The receiving antenna is a vertically polarized parabolic antenna with 39 dBi gain and 1.5^0 antenna beam width in both azimuth and elevation. They used a 200 MHz null-to-null radio frequency (RF) bandwidth, and the measurement system provided 50 PDP's per second and a multipath dynamic range of 25 dB, and the measurements were conducted in 3 different paths (LOS, partially obstructed, and obstructed path) were the transmitter and receiver were located indoors.

For the LOS case they observe that no multipath under clear conditions, however multipath was observed during rain. During moderate rain a few multipath components were detected at least 14 dB below LOS, strong multipath components were detected during heavy rain. It was observed that right before or after a hailstorm, multipath component was detected 12 dB below the LOS component. During the hailstorm, the power of LOS component was reduced by 25 dB. For the partially obstructed and totally obstructed paths a few multipath components were detected under clear conditions, and more multipath components were detected during rain events. The results form these three links indicates that severe weather conditions can change the multipath characteristics. Two hypotheses may explain the presence of multipath components during rain. The first one is based on in-homogeneities in the atmosphere. Multipath components that occurred right before and after the hailstorm may be caused by the sharp edge of the hailstorm cell, which was illuminated by the antenna main lobe or first side lobe. Pressure, temperature, and rain could alter the refractivity of the atmosphere, thus creating varying propagation paths and propagation delays. The second hypothesis is based on the change of the electromagnetic properties of the surface or the formation of standing water surfaces during rain. The rough surface on the rooftop of the building would diffusively scatter the incoming wave during dry conditions. However, if the surface becomes wet or standing water surface forms during a rain event, the reflected power in the specular direction would increase. Multipath components remained after rain, which seems to support this hypothesis.

During rain, the received signal can be modelled as the sum of a constant (coherent) component, and randomly scattered (incoherent) components resulting from rain or other scatter. Therefore, the resulting short-term received signal variation is expected to follow a Nakagami-Rice distribution. A minimum means square error (MMSE) fit is applied to the measurements, which leads to the following relationship between the Nakagami–Rice *K*-factor (dB) and rain rate *R* (mm/h)[21].

$$K = 16.88 - 0.04R \quad \text{dB} \tag{15}$$

Equation (15) shows that the *K*-factor is proportional (with a negative sign) to rain rate. This is expected because as the rain rate increases, the coherent power decreases and the incoherent scattered power increases.

5.1.4 Statistical channel description of BFWA systems

Wei Zhang [22] classified statistical channel models for BFWA systems on the basis of antenna height and directivity. When at least one of the two antennas are sufficiently high providing an LOS propagation path between the transmitter and receiver, the statistics of the BFWA radio channel should be described by one of the Nakagami-Rice, Nakagami-m, and lognormal distributions, depending on the directivity of the antennas. The channel statistics of BFWA radios using directional antennas should be characterized by lognormal or Nakagami-m distribution. A radio channel for a BFWA system using omni-directional antenna is used at least at one end of the radio link, then the channel can be evaluated by the statistics of the Nakagami-Rician distribution. When omni-directional antennas are used and at least one of the antennas is lower than the surrounding obstacles, and hence a LOS propagation path is absent, the radio channel is described by the statistics of the Rayleigh distribution.

From measurements conducted at 27.4 [1], the peak signal level variations were observed to follow Nakagami-Rice distribution with *K*-factors ranging from -4 to 12 dB. In addition, based on measurements in [1], [15], and [19] (which are discussed above), K. V. Ravi, D. Guo, K. L. Cheah [23] concluded that the BFWA channel is approximately Nakagami-Rice faded with a fairly strong specular component, so a time variant Nakagami-Rice fading channel is concluded. The parameters resulted from the channel measurements are summarised in Table 14.

Channel parameters	Suburban	Urban
Received power	-105 – -65dBm	-105 – -70dBm
Excess path loss	25 – 60 dB	40 – 65 dB
RMS delay spread	20 – 250 ns	12 – 200ns
Correlation BW	2 – 16 MHz	4 – 16 MHz
Rician *K* factor	2 – 12 dB	-4 – 12 dB
Doppler frequency	500 – 1000Hz	50 – 100Hz

Table 14. Summary of channel characteristics

5.1.4 Summary

Generally from the above different measurements and observations, the short-term received signal variation was found to follow Nakigami-Rice distribution, and the *K*-factors were found to be -4 to 12 dB for the urban, 2 to 12 dB for the suburban, and 6 to 12 for rural area [1]. Channel Doppler frequency was found to be 50 – 500 Hz for suburban and 500 – 1000 Hz for the urban case [23] and [24]. The dependency of channel multipath property on transmitting antenna beam width [20] and receiving antenna height [19] was observed, thus (transmitting/receiving) antenna beam width and

height should be considered as model parameters when developing a propagation model. The effect of antenna directivity on channel multipath property can be accounted by weighting each tap according to receiving antenna gain depending on angle of arrival of taps. We also observe the effect of different weather conditions on channel multipath property [21]. It is shown that, there is a link (relationship) between rain and multipath, more multipath was observed during rain than in clear weather conditions. The link between rain and multipath should be accounted when developing a channel model for BFWA systems.

5.2 Vegetation attenuation and fading

Vegetation effects can severely limit the performance of BFWA system operating at mm-wavelengths. Generally signals are attenuated, and in the presence of wind vegetation fading is observed. In this section signal attenuation by vegetation and signal fading due to vegetation movement because of wind are discussed.

5.2.1 Vegetation attenuation

In environment with vegetation, signals propagate through the process of scattering (propagation through vegetation), diffraction from top of vegetation and diffraction form the side of vegetation. ITU-R Rec. P.833 [25] developed an empirical model, which accounts signal attenuation through vegetation. This gives the attenuation due to propagation through vegetation as a function of the depth of vegetation, and accounts for the dual slope nature of the measured attenuation versus depth curves. The model was derived form a database of measured data over a range of frequencies 9.6 – 57 GHz, but also takes into account the site geometry, in the form of the extent of illumination of the vegetation medium, defined by the illumination width, A_{min}. The attenuation for a vegetation depth, d (meters), is given by:

$$A_{scat} = R_{\infty} d + k\left(1 - \exp\left\{\frac{-(R_0 - R_{\infty})}{k} d\right\}\right) \tag{16}$$

Here, the initial slope is:

$$R_0 = af \tag{17}$$

and the final slope is:

$$R_{\infty} = \frac{b}{f^c} \tag{18}$$

where f is the frequency (GHz) and the turnover value of attenuation, at which the scattered component of the received field becomes of the same order as the attenuated coherent component,

$$k = k_0 - 10\log_{10}\left(A_0\left(1 - \exp\left\{ \frac{-A_{min}}{A_0} \right\} \right)\left(1 - \exp\left\{ -R_f f \right\} \right) \right) \quad (19)$$

and the parameters a, b, c, k_0, R_f and A_0 are given in Table 15.

Constant Parameter	In leaf	Out of leaf
a	0.2	0.16
b	1.27	2.59
c	0.63	0.85
k_0	6.57	12.6
R_f	0.0002	2.1
A_0	10	10

Table 15. Constant values for equation (16)

A_{min}, is the minimum illumination area defined as the product of the minimum width of illuminated vegetation, $\min(w_1,w_2,w_v)$ and the minimum height, $\min(h_1,h_2,h_v)$ which corresponds to the smaller of the two antenna spot areas on the front and rear faces of the vegetation. These heights and widths are determined by the elevational and azimuthal 3 dB beam widths of the transmit antennas and the physical width, w_v, and height of the vegetation, h_v. If the transmit antenna has elevational beam width, φ_T, and azimuthal beam width, θ_T, and the receive antenna φ_R and θ_R then the minimum illumination area is defined as:

$$A_{min} = \min(h_1, h_2, h_v) \times \min(w_1, w_2, w_v)$$
$$A_{min} = \min\left(2r_1 \tan\left(\frac{\varphi_T}{2} \right), 2r_2 \tan\left(\frac{\varphi_R}{2} \right), h_v \right) \times \min\left(2r_1 \tan\left(\frac{\theta_T}{2} \right), 2r_2 \tan\left(\frac{\theta_R}{2} \right), w_v \right) \quad (20)$$

The diffraction loss for double isolated knife-edges A_{difw} due to diffraction around the sides of the vegetation and A_{difh} due to diffraction over the top of the vegetation is given in ITU-R Rec. P.526 [26]. These diffraction loses (from side and top of vegetation) are calculated by using double isolated edges. This method consists of applying single knife-edge diffraction theory successively to the two obstacles, with the top of the first obstacle acting as a source for diffraction over the second obstacle (see Figure 17). The first diffraction path, defined by the distances a, b and the height h'_1 gives a loss L_1(dB). The second diffraction path, defined by the distances b, c and the height h'_2, gives a loss L_2(dB). L_1 and L_2 are calculated using equation 21 and 22.

$$v = h\sqrt{\frac{2}{\lambda}\left(\frac{1}{d_1} + \frac{1}{d_2} \right)} \quad (21)$$

$$L(v) = 6.9 + 20\log\left(\sqrt{(v-0.1)^2 + 1} + v - 0.1\right) \quad \text{(dB)} \tag{22}$$

where h is height of the top of the obstacle above the straight line joining the two ends of the path. The distance $d_1$and d_2 are distances of the two ends of the path from the top of the obstacle, v is a lost parameter and $L(v)$ gives the diffraction lost. Correction terms L_c (dB) must be added to take into account the separation b between the edges. L_c may be estimated by the following formula:

$$L_c = 10\log\left[\frac{(a+b)(b+c)}{b(a+b+c)}\right] \tag{23}$$

which is valid when each of L_1 and L_2 exceeds about 15 dB. The total diffraction loss is then given by:

$$L = L_1 + L_2 + L_c \tag{24}$$

This method is particularly useful when the two edges give similar losses.

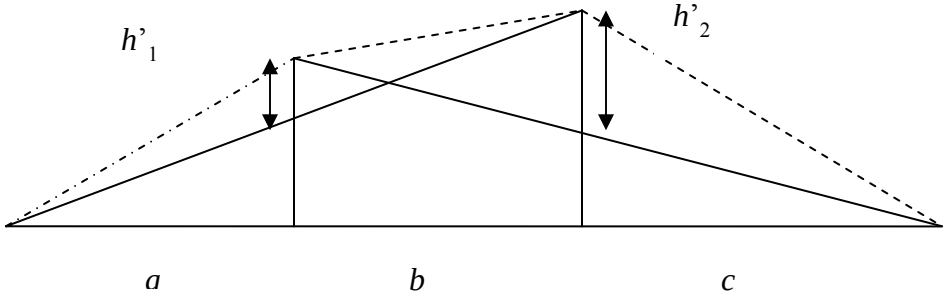

Figure 17. Method for double isolated edges

Other empirical model for attenuation by foliage was reported in [27] and it is given by:

$$A_m = 0.5 f^{0.75} \tag{25}$$

where A_m the one-way attenuation level in dB/m and f is the frequency in GHz. Further measurements at 42 GHz have been made in Norway to study signal attenuation by vegetation [20]. From the measurements it was observed 5 dB attenuation of signal per meter depth behind the vegetation. The general trend of the measurements is for the

attenuation to increase as the receiver is lowered below the treetops. However, this attenuation mentioned above is an averaged value, and the signal itself may vary rapidly with time, making the service extremely unreliable. A receive site may occur where one or more trees encroach on the signal path, but do not give a sufficient mean attenuation to take the received signal level below the system margin. However, as the trees move because of wind effects, the signal level may vary sufficiently to knock out the signal for short periods of time.

5.2.2 Vegetation fading

The raped movement of vegetation due to wind results in signal fading. In order to model the dynamic vegetation effects, statistical knowledge of signal attenuation by vegetation is needed. A number of measurements and studies have been conducted in order to describe this statistics. N. Naz, D. D. Falconer [6] conducted measurements at 29.5 GHz, where a temporal variation due to foliage movements due to wind, and because of passing vehicles was studied. The measurements were taken at 2000 samples per second in order to observe the signal variation because of foliage movement due to wind and passing vehicles. Two scenarios have been observed and analyzed in detail. These are temporal variations because of foliage movements due to wind and temporal variations because of passing vehicles. For scenarios with trees between the transmitting and receiving antennas, the following observations were noted:

- The dependence of fading characteristics on different types of trees.
- Heavy dense trees cause attenuation but do not produce much variation.
- Trees with green foliage (in summer) produce less variation as compared to trees with yellow and dehydrated foliage (in fall)
- Variation due to foliage is a continuous process. Signal continuously varies in a certain range.
- Evergreen trees when disturbed by wind produce slow fading, while deciduous trees produce faster fading.
- Fade depth due to trees is less than the variation due to passing vehicles. This is probably because of the attenuation of the foliage.

An attempt was also made to fit the acquired data to theoretical statistical model; Nakagami-Rice distribution was found to best fit the acquired data (95%). Doppler bandwidth for an average fading of 40 dB because of foliage movement was found to be 500Hz, and in other similar study it was found that the Doppler spectrum might be characterised as a single pole response at 100 Hz for windy conditions [28].

From other studies at 28 GHz by M. Polo Chavero, V. Ramos and F. Marti [29], the Nakagami-Rice distribution was found to best represent signal attenuation through vegetation. Akihiro Kajiwara [30] studies the dynamic effect of vegetation, where he investigates an obstructed radio channel by foliage for BFWA where a relative evaluation of attenuation characteristics of foliage at 29.5 and 5 GHz is performed. In his study two different types of foliated trees (summer plane and ginkgo) were selected and 5 branches

of each tree were bundled loosely to imitate the treetop, thereby the effect of swaying foliage in wind could be evaluated quantitatively using an electric fan in an anechoic room. The results obtained are summarized as follows.

In obstructed channel by foliage, swaying foliage in wind causes a significant channel fading at 29.5 GHz, and temporal variation of the attenuation at 29.5 GHz is much larger than that for 5 GHz. The fading depth is approximately 15 dB, which depends on the direction and velocity of wind, tree species, foliage density, humid climate and very complex leaf structure, and it is much larger than that for 5 GHz. This is because the motion of leaves is comparable to a wavelength of 29.5 GHz, thereby resulting in a significant effect on the obstructed channel. It has also been found that the attenuation level in dB is likely to fit Nakagami-Rice distribution with K= 4 in the case of 29.5 GHz, and K=1 in the case of 5 GHz, where generally the K- factor is likely to depend on the leaf size, the total area of leaves and humid climate. Table 16 summarizes attenuation characteristics of swaying foliage (mean E[A], standard deviation σ_A, and attenuation level in dB)

(a)

Plane foliage		Soft wind (1.5m/s)	Fair wind (2.4m/s)	High wind (3.4m/s)
29.5 GHz	E[A] dB	20.7	21.8	22.2
	σ_A dB	3.7	4.1	3.1
5 GHz	E[A] dB	6.6	7.0	7.4
	σ_A dB	0.8	0.8	0.6

(b)

Ginkgo foliage		Soft wind (1.5m/s)	Fair wind (2.4m/s)	High wind (3.4m/s)
29.5 GHz	E[A] dB	7.3	7.6	8.0
	σ_A dB	1.4	1.5	1.4
5 GHz	E[A] dB	3.5	3.6	3.7
	σ_A dB	0.5	0.6	0.4

Table 16. Attenuation characteristics of swaying foliage in wind

It appears that the fading depth increases with the operating frequency, important results of this study include that swaying foliage causes more significant fading at higher frequency. Similar conclusions on the statistical attenuation distribution where made in reference [15] where narrowband measurement was made to study area coverage, short-term time variations of the signal, depolarisation and cell-to-cell coverage. From the measurements a significant attenuation caused by the tree canopy extending above roof height was observed. This vegetation canopy attenuates the LOS signal from the transmitter and cause signal degradation in form of attenuation, multipath and depolarisation. They observed that the K-factors were found to be a good measure of

channel variability, however the Nakagami-Rice distribution produced deeper fades than were observed from the measurement.

M. H. Hashim and S. Stavrou [4] made similar study at 17 GHz. From their study the best fit was obtained with a Nakagami-Rice distribution, with a *K*-factor exponentially decreasing with wind speed. This is because, due to the nature of the thin and sparsely distributed leaves and branches of the sample trees used in the experiments, a strong dominant signal contribution was expected to be present in the received signal superimposed with random multipath contributions, caused by scattering and multiple reflections within the tree structure. The dominant signal component was assumed to be composed of attenuated direct signal and contributions from transmission around the sample tree. Therefore, PDF of the fast fading amplitude was thought to follow a Nakagami-Rice distribution. However, as the wind speed increases, increment in random multipath power contributions was expected, which would then shift the PDF toward a Rayleigh distribution.

Even through a number of studies conclude a Nakagami-Rice distribution best models the signal attenuation through vegetation, Simon Perras and Luc Bouchard [31] form their study on fading characteristics of radio frequency (RF) signals due to foliage in frequency bands from 2 to 60 GHz concluded that the extreme value and lognormal models best represent RF attenuation characteristics through trees. The lognormal distribution gave the bets fit to measurements for low attenuation values, and the extreme value distribution gave better results for the large attenuation values in the tail of the distribution.

CRABS [20] studied the dynamic vegetation effects. Several measurements of signal level through trees as a function of time at 42 GHz has been done, and shows an average reduction of the signal level by about 20 dB, with occasional fades as deep as 50 dB below the LOS value, with duration of the order of 10 ms. It was observed vegetation dynamics due to wind causes significant channel fading. In order to simulate this propagation mechanism, the summed field from a number of scattering sources randomly positioned along a line tangential to the path has been calculated. To give the resultant signal suitable time variability, the position of each scatters was varied sinusoidally to simulate the movement of tree branches in the wind. The frequency and extent of the position variability was increased with increasing wind speed. Based on these measurements the ITU-R Rec. P.1410 [32] developed a linear model between standard deviation and wind speed.

$$\sigma = \frac{v}{4} \quad \text{dB} \tag{26}$$

where v is wind velocity in m/s. Figure 18 shows the CRABS measurements, CRABS model and ITU-R P.1410 linear model.

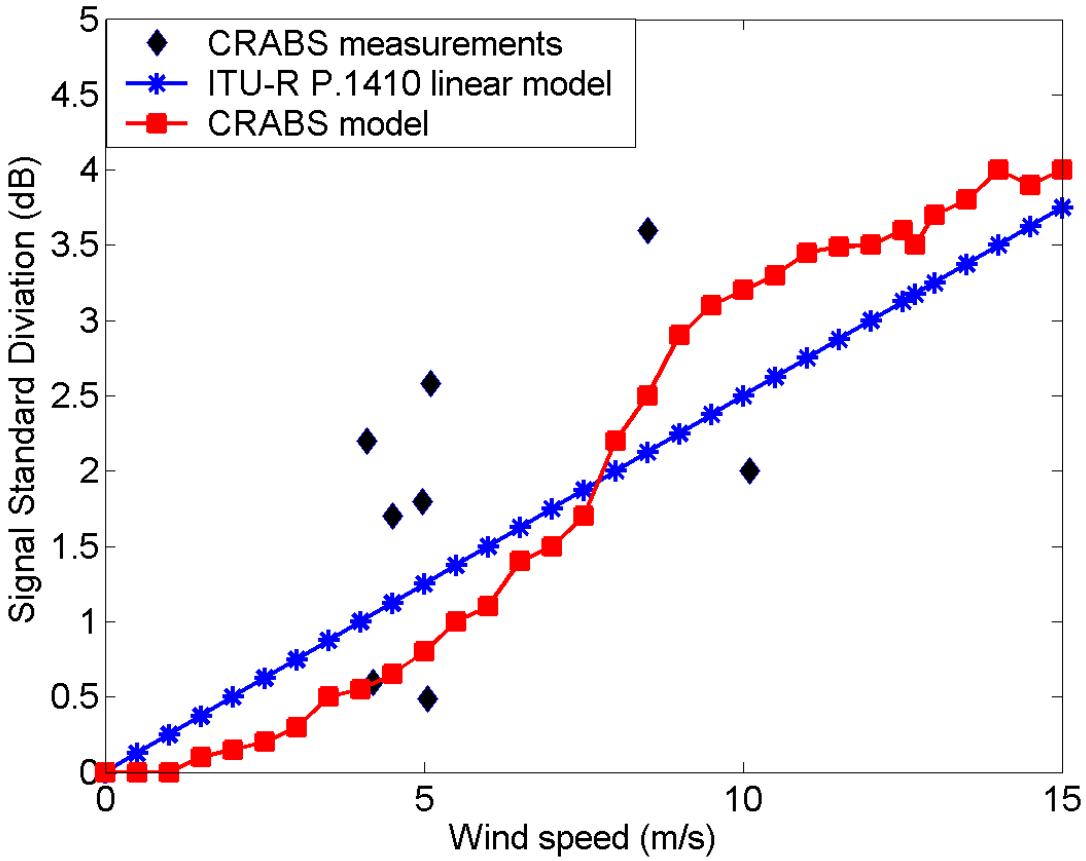

Figure 18. Standard deviation verses wind speed

We observe from Figure 18 that increasing wind speed increases the standard deviation (dynamics). Generally it was observed that the effect of vegetation affects only the received signal power not the multipath characteristic of the channel [33].

5.2.3 Summary

In this section we studied the effect of vegetation on BFWA system operating at mm-wavelengths. It was observed that vegetation effects are higher for high frequencies than for the low frequencies [30]. It was also observed that vegetation dynamics due to wind causes significant channel fading. Generally it was observed that the effect of vegetation affects only the received signal power not the multipath characteristic of the channel [33]. This means that vegetation has almost no effect on the delay spread, and we need to concentrate only on the signal attenuation and signal variation caused by vegetation. From the above discussions we observe that most of the studies conclude Nakagami-Rice distribution that best represents the dynamic vegetation attenuation [4] [6] [15] [29] [30]. The Doppler bandwidth for an average fading of 40 dB because of foliage movement was found to be 500 Hz [6], and in other similar study it was found that the Doppler spectrum might be characterised as a single pole response at 100 Hz for windy conditions [28]. The measurement results, which are summarized in this section, are essential when developing a time dynamic vegetation attenuation model.

5.3 Dynamics of precipitation attenuation

Precipitation (rain, snow, fog, hailstorm, etc) affects the characteristics of propagating signal. Under these weather conditions the signal is attenuated, and in the case of rain, signal attenuation and depolarisation is observed. The multipath effect of rain is discussed in section 5.1.3 taken from [21]. In this section we concentrate on the dynamic effect of rain attenuation on radio signals.

5.3.1 Rain attenuation

Attenuation by rain can occur as a result of absorption and scattering, and the dynamical variation is caused by the temporal and spatial changes of the precipitation. Rain attenuation must be accounted at frequency range of interest and above about 10 GHz its importance increases rapidly with frequency. ITU–R Rec. P.530 [34] provides a simple technique for estimating the long-term statistics of rain attenuation. The following steps are taken to find the rain attenuation:

Step 1: Obtain the rain rate $R_{0.01}$ exceeded for 0.01% of the time (with an integration time of 1 min).

Step 2: Compute the specific attenuation, γ (dB/km) for the frequency, polarization and rain rate of interest using Recommendation ITU-R P.838 [35]. The specific attenuation γ (dB/km) is obtained from the rain rate R (mm/h) using the power-law relationship [35]:

$$\gamma = kR^{\alpha} \tag{27}$$

The frequency-dependent coefficients k and α are given in Table 17 for linear polarizations (horizontal: H, vertical: V) and horizontal paths. Values of k and α at frequencies other than those in Table 17 can be obtained by interpolation using a logarithmic scale for frequency, a logarithmic scale for k and a linear scale for α.

For linear and circular polarization, and for all path geometries, the coefficients in equation (27) can be calculated from the values in Table 17 using the following equations:

$$k = \left(k_H + k_V + (k_H - k_V)\cos^2\theta\cos 2\tau\right)/2 \tag{28}$$

$$\alpha = \left(k_H\alpha_H + k_V\alpha_V + (k_H\alpha_H - k_V\alpha_V)\cos^2\theta\cos 2\tau\right)/2k \tag{29}$$

where θ is the path elevation angle and τ is the polarization tilt angle relative to the horizontal ($\tau = 45°$ for circular polarization).

Step 3: Compute the effective path length, d_{eff} of the link by multiplying the actual path length *d* by a distance factor *r*. An estimate of this factor is given by:

$$r = \frac{1}{1 + d / d_0} \tag{30}$$

Where, for $R_{0.01} \leq 100$ mm/h:

$$d_0 = 35e^{-0.015R_{0.01}} \tag{31}$$

For $R_{0.01} > 100$mm/h, use the value 100 mm/h in place of $R_{0.01}$

Step 4: An estimate of the path attenuation exceeded for 0.01% of the time is given by:

$$A_{0.01} = \gamma \cdot d_{eff} = \gamma \cdot dr \qquad \text{(dB)} \tag{32}$$

Step 5: For radio links located in latitudes equal to or greater than 30^0 (North or South), the attenuation exceeded for other percentages of time *p* in the range 0.001% to 1% may be deduced from the following power law:

$$\frac{A_p}{A_{0.01}} = 0.12\, p^{-(0.546+0.043\log_{10} p)} \tag{33}$$

This formula has been determined to give factors of 0.12, 0.39, 1 and 2.14 for 1%, 0.1%, 0.01% and 0.001% respectively, and must be used only within this range.

Step 6: For radio links located at latitudes below 30^0 (North or South), the attenuation exceeded for other percentages of time *p* in the range 0.001% to 1% may be deduced from the following power law:

$$\frac{A_p}{A_{0.01}} = 0.07\, p^{-(0.855+0.139\log_{10} p)} \tag{34}$$

This formula has been determined to give factors of 0.07, 0.36, 1 and 1.44 for 1%, 0.1%, 0.01% and 0.001%, respectively, and must be used only within this range.

Step 7: If worst-month statistics are desired, calculate the annual time percentages *p* corresponding to the worst-month time percentages p_w using climate information specified in Recommendation ITU-R P.841 [36]. The values of *A* exceeded for percentages of the time *p* on an annual basis will be exceeded for the corresponding percentages of time p_w on a worst-month basis.

The prediction procedure outlined above is considered to be valid in all pars of the world at least for frequencies up to 40 GHz and path length up to 60 km.

Frequency (GHz)	k_H	k_V	α_H	α_V
1	0.0000387	0.0000352	0.912	0.880
2	0.000154	0.000138	0.963	0.923
4	0.000650	0.000591	1.121	1.075
6	0.00175	0.00155	1.308	1.265
7	0.00301	0.00265	1.332	1.312
8	0.00454	0.00395	1.327	1.310
10	0.0101	0.00887	1.276	1.264
12	0.0188	0.0168	1.217	1.200
15	0.0367	0.0335	1.154	1.128
20	0.0751	0.0691	1.099	1.065
25	0.124	0.113	1.061	1.030
30	0.187	0.167	1.021	1.000
35	0.263	0.233	0.979	0.963
40	0.350	0.310	0.939	0.929
45	0.442	0.393	0.903	0.897
50	0.536	0.479	0.873	0.868
60	0.707	0.642	0.826	0.824
70	0.851	0.784	0.793	0.793
80	0.975	0.906	0.769	0.769
90	1.06	0.999	0.753	0.754
100	1.12	1.06	0.743	0.744
120	1.18	1.13	0.731	0.732
150	1.31	1.27	0.710	0.711
200	1.45	1.42	0.689	0.690
300	1.36	1.35	0.688	0.689
400	1.32	1.31	0.683	0.684

Table 17. Regression coefficients for estimating specific attenuation in equation (27)

5.3.2 Dynamic rain attenuation

The dynamical variation of rain attenuation is caused by the temporal and spatial changes of the precipitation. It has been shown that the attenuation of a microwave radio signal caused by rain has a lognormal stationary distribution [37]. In the planning of communication systems, the dynamic properties of rain attenuation are also of interest, this is because the channel doesn't remain static in the presence of rain; thereby dynamic rain attenuation models are needed.

Masseng and Bakken [2] developed a dynamic rain attenuation model. The model transforms the attenuation α (in dB) into a Gaussian stationary Markov process of the Ornstein-Uhlenbeck type sees Figure 19. The model consists of two successive parts, a filtering step to reflect the dynamic behaviour of the attenuation due to rain and a normalization step to be in agreement with the long-term distribution of rain attenuation.

$$x(t) = \frac{\ln(\alpha(t)/\alpha_m)}{\sigma_a} \tag{35}$$

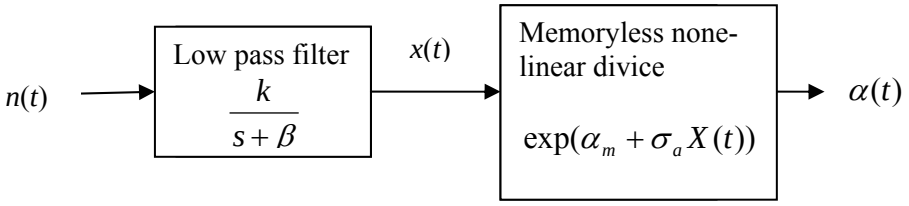

Figure 19. Rain attenuation model

Were α_m is the median attenuation, σ_a is the standard deviation of $\ln(\alpha)$. The first order Markov process implies that, given the rain attenuation at a time *t*, the model allows statistics to be generated for future rain attenuation, and these statistics cannot be improved upon by consideration of the rain attenuation prior to *t*. The model allows the stationary distribution function of rain attenuation to be described by median attenuation α_m and standard deviation σ_a. The time dependence is described by a single parameter β (rate of change of attenuation), which is used in a first order infinite impulse response filter to shape the autocorrelation function (ACF). This ACF is assumed to have a relatively simple shape of a decaying exponential function corresponding to an auto regressive process of first order.

$$R_{XX}(\tau) = e^{(-\beta|\tau|)} \tag{36}$$

A small value of β corresponds to slowly varying rain attenuation dynamics. Reference [38] rapports values for β, this is reproduced in Table 18.

Event	Median	Standard dev	β (10^{-3})/s	Date
1	2.47	1.11	9.22	Oct. 95
2	0.84	1.37	6.45	Sept. 95
3	1.82	1.31	8.50	July 95
4	5.04	0.99	2.37	July 95
5	4.35	1.21	3.41	July 95
6	4.33	1.32	3.57	July 95
7	2.45	1.20	14.04	June 95
8	3.22	1.00	1.95	June 95
9	3.17	0.88	1.63	June 95
10	2.07	1.23	18.45	Sept. 94
11	4.10	1.26	2.92	Aug. 94
12	4.65	1.20	1.46	Aug. 94
Mean	2.96	1.08	5.69	

Table 18. Rain events and extracted parameters for *x*(*t*)[38]

When these three parameters have been determined, the properties of interest, such as the autocorrelation function for the rain attenuation and the complete transition probability density may be found by calculation. This model is applicable only during the rain periods because no dynamic transition mechanism between rainy weather and clear sky conditions has been incorporated.

A generalization of the Maseng and Bakken model [2] which is extended to model; 1) the long term power spectral density of rain attenuation; 2) rain fade slope; 3) rain frequency scaling factor; 4) site diversity; and 5) fade duration statistics using a novel method based on Markov Chains, is reported by Boris Christian and Miodrag Filip[3]. The long-term power spectral density of rain attenuation is found to be:

$$P^{\infty}(w) \approx \frac{2\beta \cdot \sigma^2 \cdot e^2 \cdot e^{2m} \cdot e^{2\sigma^2}}{w^2}, w > w_c \tag{37}$$

$$P^{0}(w) \approx 0.1745 \cdot \frac{e^{2m} \cdot e^{\sigma^2} \cdot e^{2.648\sigma}}{\beta}, 0 < w \le w_c \tag{38}$$

$$w_c \approx 3.3855 \frac{\beta \cdot \sigma \cdot e^{\sigma^2/2}}{e^{1..324 \cdot \sigma}} \tag{39}$$

This expression shows that the asymptotic PSD of rain attenuation has a first-order low-pass characteristic. Furthermore, the space-time parameter β will affect the whole shape of the spectrum. The cut-off frequency w_c rad/s is independent of the median value e^m of rain attenuation. This gives an easy way to identify a value of the dynamic factor β for particular events (or average PSD on a long-term basis). For this, one needs to compute the PSD of rain attenuation showing clearly the cut-off frequency. The variance of the event can be estimated for this particular event in the time domain from which β can be calculated using the inverted form of equation (39). From measurements the value of β was found to be 3.16 x $10^{-4} \le \beta \le$ 3.16 x 10^{-3}, with a central value of $7.9 \times 10^{-4} s^{-1}$. The variation in the results indicates that dynamic parameter β depends on local climate as well as the form of precipitation at one location.

5.3.3 Summary

The long-term rain attenuation was found to have a lognormal distribution [37]; therefore lognormal distribution can be used to model the rain attenuation. There exist models that model the dynamic rain attenuation (for example Maseng and Bakken [2] and Boris Christian and Miodrag Filip [3]). Both models require knowledge of average rain attenuation α_m, standard deviation σ_a, and time dynamics β. The value of the average rain attenuation and standard deviation may be derived from either local measurements of attenuation distribution or estimated attenuation distribution from ITU-R Rec. P.530 [34] by applying curve-fitting routines (for example Matlab).

6 Time dynamic channel model for BFWA systems

The objective of this study is to understand the radio propagation characteristics at mm-wave and develop a realistic time dynamic channel model for BFWA systems operating above 20 GHz. By combining the effects of rain, vegetation and multipath, a realistic time dynamic wideband channel model has been developed. In this section we first describe the adapted dynamic rain attenuation model and then the developed dynamic models for vegetation and multipath. These individual models are then combined to give a time dynamic channel model for BFWA systems operating above 20 GHz, accountin for the effect of rain, vegetation and multipath. Figure 20 shows the major propagation effects that are considered in the developed channel model. An input signal $x(t)$ is attenuated by time varying rain and vegetation, and also affected by time varying frequency selective fading.

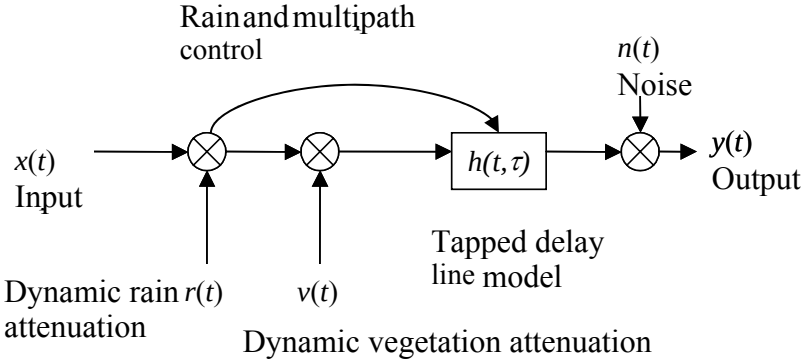

Figure 20. Time dynamic BFWA channel model

A link between rain attenuation and multipath severity is shown in Figure 20. More severe multipath has been observed during rain compared to clear air weather conditions (more discussions on this are found in Section 5.2 taken from reference [21]). A model that controls this relationship is found in Section 6.3.

6.1 Dynamic rain attenuation model

In the proposed combined channel model, the Maseng-Bakken statistical dynamic model of rain attenuation is adapted from [2]. The received signal attenuation α (in dB) is modelled as a log-normally distributed variable. The value of the average rain attenuation and standard deviation may be derived from either local measurements of attenuation distribution or estimated attenuation distribution from ITU-R Rec. P.530 [34] by applying curve-fitting routines. The mean square error of *ccdf* of estimated rain attenuation and *ccdf* of lognormal distribution are minimised to give the best fit. The time dependence is described by the parameter β, which is used in a first order infinite impulse response filter to shape the auto correlation function, and it is found from measurements to be centred on

$7.9\times10^{-4}\,s^{-1}$ [3]. Detailed discussions on the Maseng-Bakken model are found in Section 5.3.2, taken from [2].

Figure 21 shows the curve fitting routine used to minimise the mean square error of lognormal *ccdf* and rain *ccdf* implemented in Matlab. Figure 22 shows simulated dynamic rain attenuation with a samplings rate of 10 Hz, assuming a rain rate of 30 mm/h at 0.01 percent of time, resulting in an attenuation at 0.01 percent of time of 15.66 dB for a 2 km length path (estimated from ITU-R Rec. P530 [34]) with $\beta = 7.9\times10^{-4}\,s^{-1}$. The optimised lognormal parameters that give best fit between *ccdf* of estimated rain attenuation and *ccdf* of lognormal distribution are -4.9388 and 2.9956 for the mean and standard deviation of lognormal distribution respectively.

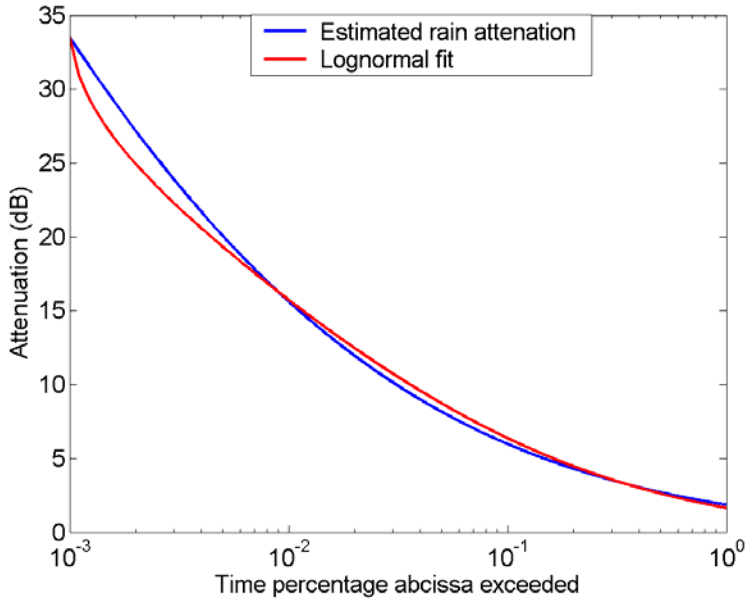

Figure 21. Curve fitting, between lognormal *ccdf* and estimated rain attenuation *ccdf*

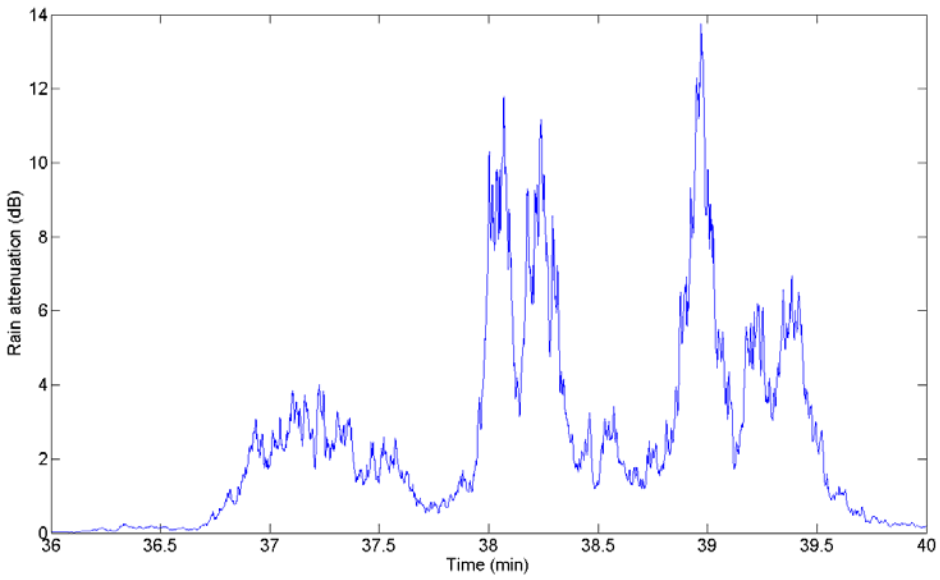

Figure 22. Dynamic rain attenuation time series

Based on the BFWA system layout, example distances between transceivers and local rain rate and rain dynamics statistics; this time dynamic rain attenuation model can be incorporated into system level simulations together with other propagation degradations such as scintillation, multipath and vegetation attenuation.

6.2 Dynamic vegetation attenuation model

Vegetation effects can severely limit the performance of BFWA system operating at mm-wavelengths. Attenuation due to single trees varies significantly with species, whether trees are in leaf or wet [39]. At frequencies above 20 GHz leaves and needles have dimensions large compared to wavelength and will significantly affect the propagation conditions. A theoretical description of penetration into vegetation is given by the theory of radiative energy transfer. Range dependence of vegetation attenuation is characterised by high attenuation at short vegetation depths and a reduced attenuation rate at larger depth due multiple scattering causing beam broadening and depolarisation [40]. The transition between the two regimes can be rather abrupt and the change in attenuation rate substantial. Due to limited power margin in operational BFWA systems, the first regime is most interesting. In this regime, the received signal consists of the coherent components attenuated direct wave, diffracted and ground reflected waves in addition to the diffuse component resulting from scattering within the foliage. Measurements reported in [41] showed that diffraction around the tree is the dominant mode of propagation for trees in leaf with only a weak scattered component. For trees without leaves the ground reflected component dominated.

A number of measurements were done in order to study the effect of vegetation and its statistical description, more discussions on this are found in Section 5.2.2. There are significant variations between the different measurement campaigns with respect to the best choice of theoretical attenuation distribution function; however, the majority of the experimental results seem to indicate that the Nakagami-Rice distribution is suitable for general modelling usage [4] [6] [15] [29] [30]. This implies that the coherent component propagation through and diffracting around, the vegetation is considered constant. The PDF of the Nakagami-Rice attenuation distribution for the envelope v is

$$p(v) = \frac{v}{\sigma^2} e^{-\left(v^2+a^2\right)/2\sigma^2} I_0\left(\frac{va}{\sigma^2}\right) \tag{40}$$

where I_0 is the modified Bessel function of zero order. The relation between the coherent components amplitude, a, and the power in the diffuse component, $2\sigma^2$, may be expressed by the Nakagami-Rice factor $K = 10 \cdot \log_{10}\left(a^2 / 2\sigma^2\right)$. The average total received power can be determined from ITU Rec. P.833 on vegetation [25].

It was observed from 12 and 17 GHz measurements reported in [4] that the K-factor decreases exponentially as wind speed increases see Figure 24. The CRABS project reported measurements of signal level standard deviation at 42 GHz [20], leading to the linear model between standard deviation and wind speed in ITU-R Rec. 1410 [32]. The

standard deviation produced by the Nakagami-Rice model was compared to that of ITU-R P.1410 model as function of wind speed, and a good agreement was obtained between the models, see Figure 23.

Figure 24 shows the variation of Nakagami-Rice *K*-factor as a function of wind speed for three different frequencies. By estimating the average vegetation attenuation at 42 GHz according to ITU-R P.833 [25], and then assuming a Nakagami-Rice distributed envelope and a variation of the *K*-factor according to Figure 24, we get a resulting vegetation time series as shown in Figure 25 and 26. The mean vegetation attenuation is 12.6 dB for the 42 GHz signal, the sampling rate is 200 Hz, and the dynamics of the Gaussian processes is controlled by utilising a first order Butterworth filter with a 3 dB cut-off frequency of 1.5 Hz, resulting in a 40 dB cut-off frequency of about 50 Hz, comparable to the results reported in [31], [5] and [28].

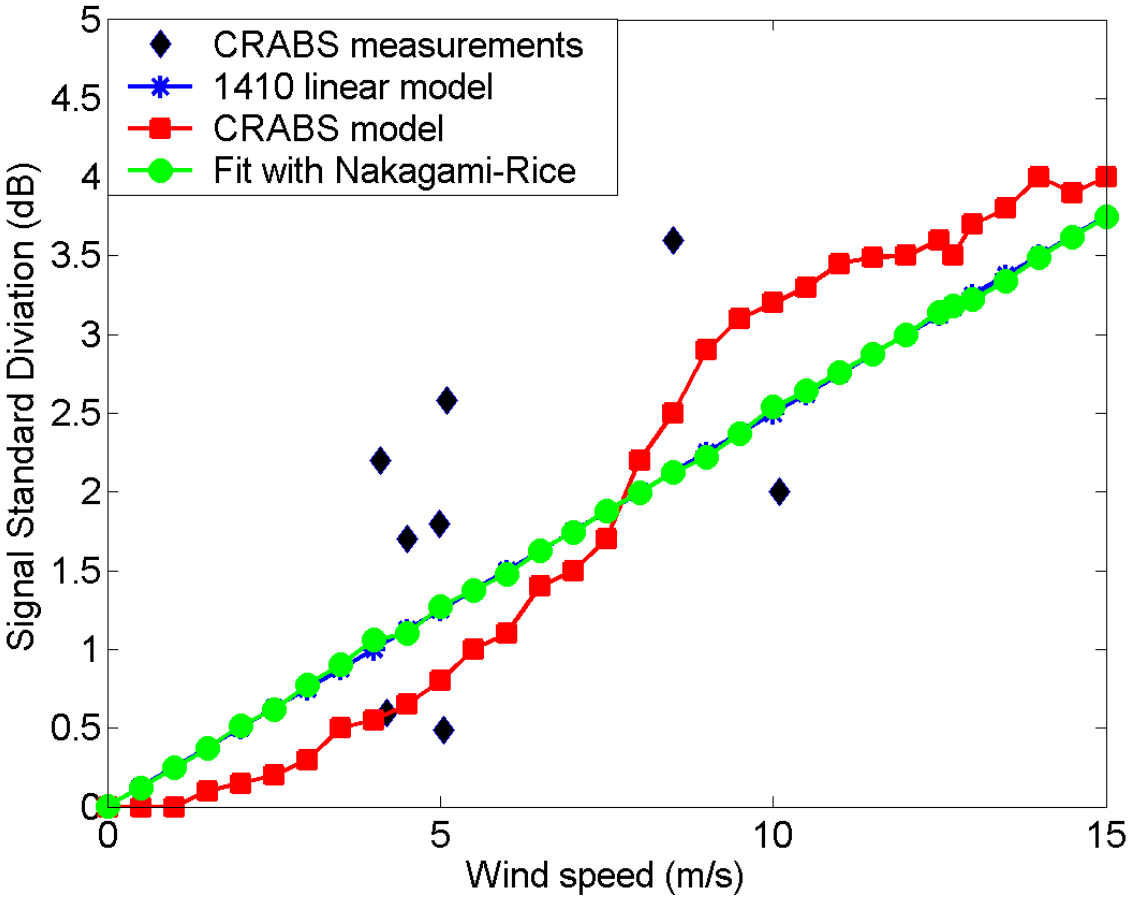

Figure 23. Signal standard deviation as a function of wind speed. Comparison between CRABS measurements, CRABS model, ITU-R P.1410 linear model, and fit with Nakagami-Rice (our proposed new model)

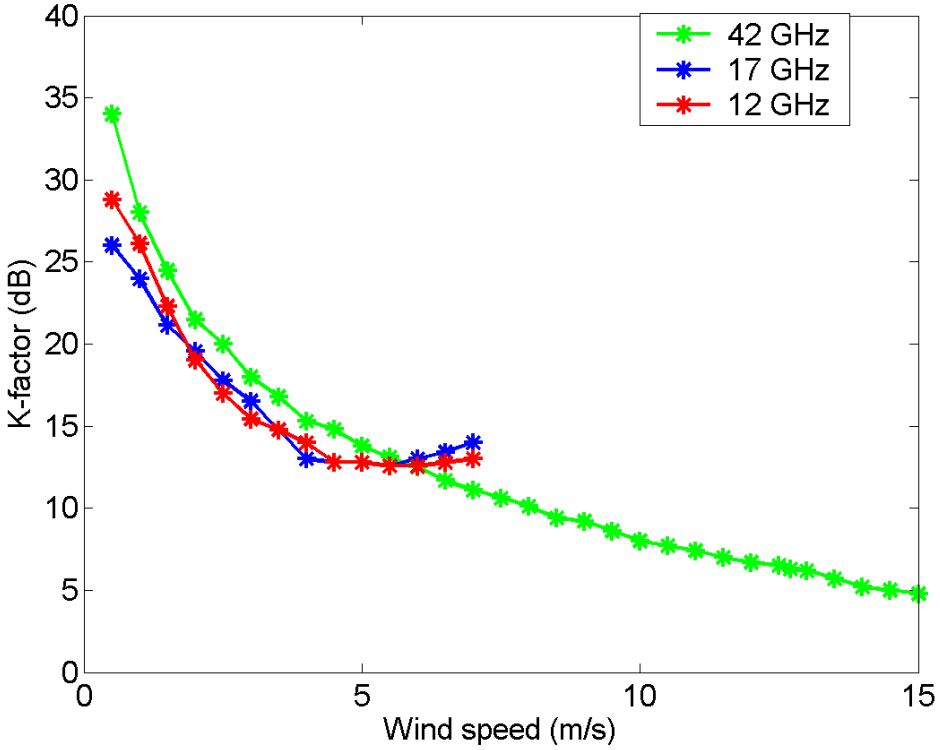

Figure 24. Nakagami-Rice *K*-factor as function of wind speed
17 and 12 GHz from [4], 42 GHz derived from Figure 23

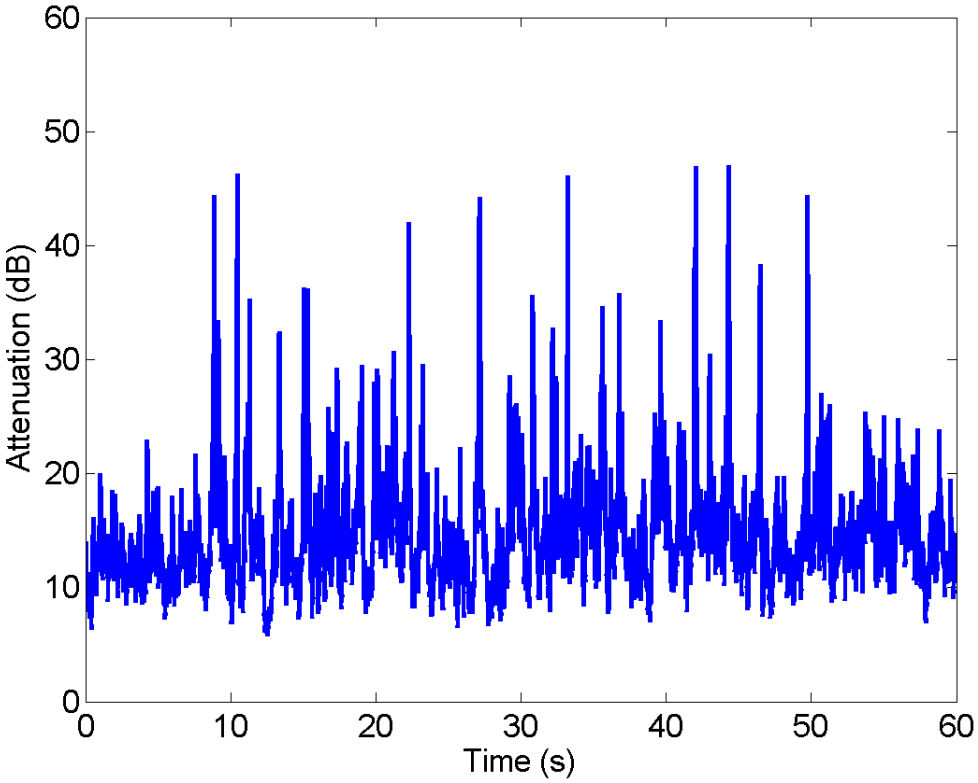

Figure 25. Dynamic vegetation attenuation time series
In leaf, K = 3 dB, which corresponds over 15 m/s wind speed

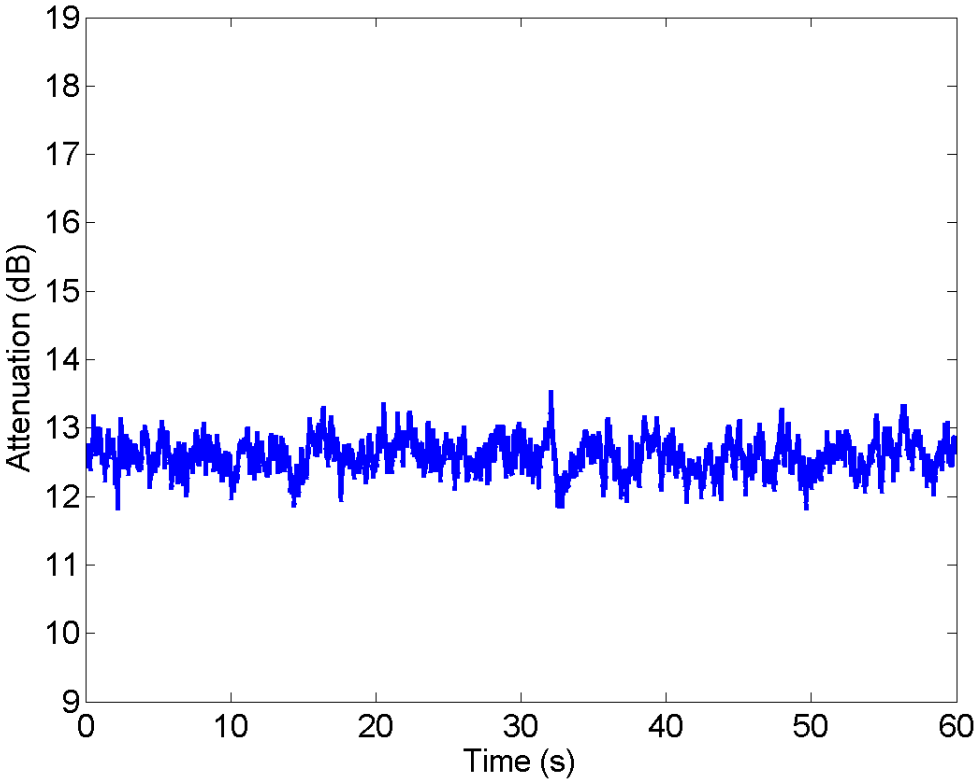

Figure 26. Dynamic vegetation attenuation time series
In leaf, K = 28 dB, which corresponds to 1 m/s wind speed

From discussions in this section, we conclude that the developed Nakagami-Rice model for dynamic vegetation attenuation is in good agreement with existing models link ITU-R P.1410 [32], see Figure 23.

6.3 Generic tapped delay line model

Multipath propagation causing frequency selective fading may become significant when the system bandwidth exceeds the channels coherence bandwidth. The time delays between the multipath components depends on both the surrounding reflectors and the antennas involved, imposing a distinction between propagation paths between base stations and propagation paths from a base station to the users. Depending on the antennas utilised, and the transmission environment, multipath components with significant delay spreads will occur. To enable interference estimation and simulations of interference reduction techniques we define the time varying channel impulse response $h(t,\tau)$:

$$h(t,\tau)=\sum_{n=0}^{N-1} m(t,n)\delta(t-\tau_n)e^{-j(\omega_c\tau_n+\varphi_n(t))} \tag{41}$$

where n is the tap index, N is the number of taps, ω_c is the carrier angular frequency, τ_n is the excess delay of each multipath component, $\varphi_n(t)$ is the phase for tap number n within the range $[0,\ 2\pi]$, and $m(t,\ n)$ denotes the time varying envelope for tap number n.

Normally m is normalised to obtain a unit channel gain. Wideband 200 MHz channel measurements at 38 GHz in a campus environment were reported in [21], multipath on a LOS link was only observed during rain and hail, not during clear weather. This may be due to changes in electromagnetic properties of the buildings and vegetation as the scattering surfaces becomes wet. This is supported by the increased multipath activity on the two partly obstructed paths during rain. After the surfaced dried up, the multipath power decreased. More discussions on the effect of rain on multipath property of the channel are found in Section 5.1.3 taken from [21]. The short-term variation in signal strength over 1-2 minutes was well described by a Nakagami-Rice distribution with a Nakagami-Rice K-factor depending on the rain intensity R (mm/h) [21]. For convenience, equation 15 that gives the link between Nakagami-Rice K-factor (dB) and rain rate R (mm/h) is repeated below.

$$K = 16.88 - 0.04R \quad \text{(dB)} \tag{42}$$

The time varying rain rate R(t) can be estimated from rain attenuation time series by using equation 27, taken from [35], repeated below for convenience:

$$\gamma = kR^{\alpha} \quad \text{(dB/km)} \tag{43}$$

where R is the rain rate, γ is specific rain attenuation, k and α are frequency-dependent coefficients given in Table 17 [35]. After estimating the time varying rain rate R(t), equation 42 is then used to get the time varying Nakagami-Rice K-factor K(t). We may choose the main scattered component (specular reflection or LOS component) according to a given Nakagami-Rice K-factor and let the remaining taps follow Nakagami-Rice distributions with a K-factor decreasing with average tap power. In the simulations we have used ΔK = -5 dB (decrementing factor) between the taps. The path occurrence process may be modelled as a modified Poisson renewal process taking into account that paths tend to arrive in time clusters [42]. For simplicity, however, we have assumed a uniform spacing between the taps in our model. Depending on the signal bandwidth and the maximum tap delay, which in turn depends on the type of environment (urban, suburban and rural), the model generates taps with average tap power given by:

$$P = \exp(-3\tau_n / \tau_{\max}) \tag{44}$$

where τ_n is the tap delay and $\tau_{\max}$ is the maximum tap delay. The maximum delay is a random function that depends on the environment type and the type of transceiver antennas (transmitter: sector or omni-directional antenna, receiver: narrow beam or wide beam antenna), measurements from [1] reported a maximum delay of 400 ns in the urban case. Filtering the Gaussian processes, as for vegetation, controls the dynamics and we have assumed the same filtering bandwidth and sampling frequency. The resulting power delay profile and tap time series are shown in Figure 27 and 28 respectively.

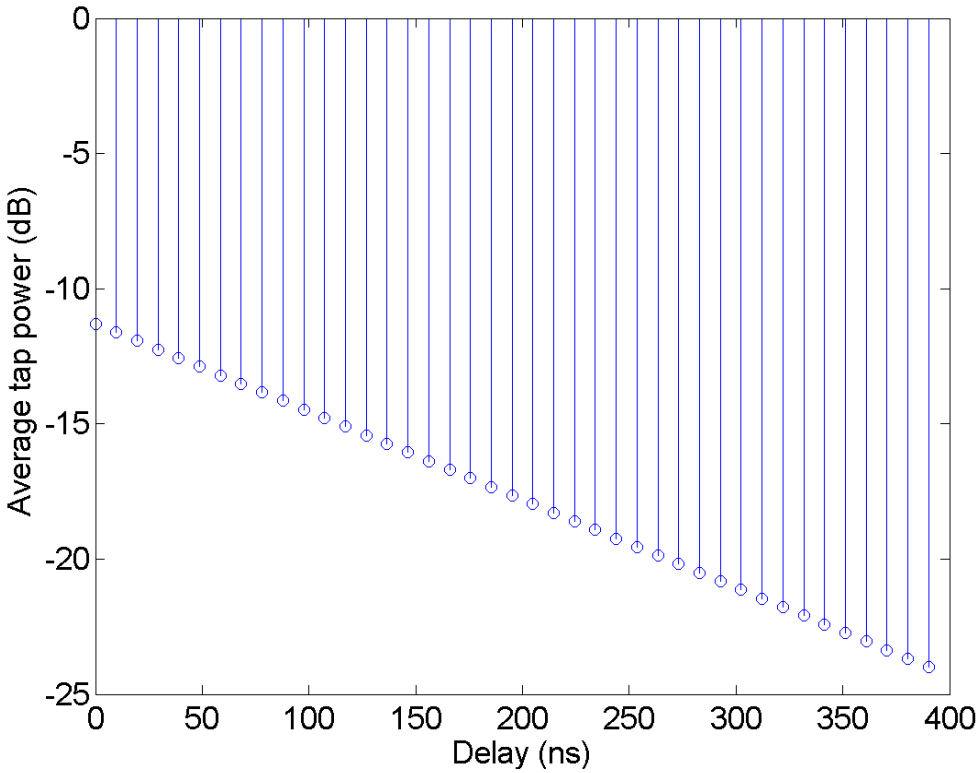

Figure 27. Power delay profile with maximum tap delay of 400 ns

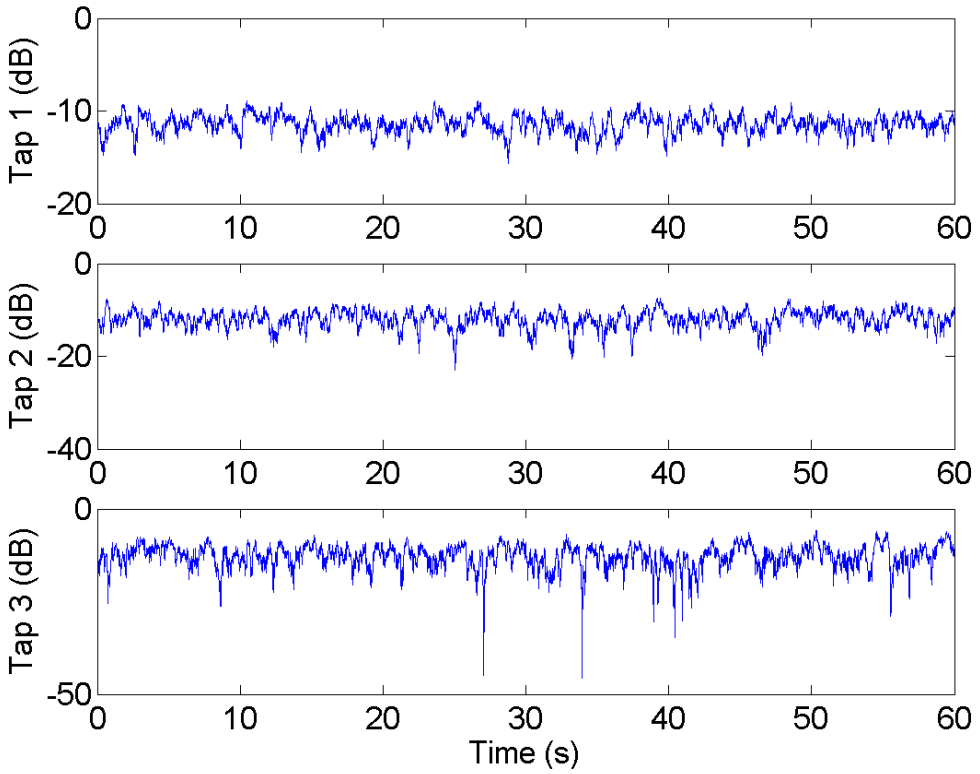

Figure 28. Tap envelopes of the first 3 taps

6.4 Combined dynamic channel model

The individual dynamic models for rain, vegetation and multipath are combined to give one realistic channel model, which accounts the effect of rain, vegetation and multipath as shown in Figure 20. The sampling rate of rain (10 Hz) is interpolated to be equal to sampling rate of vegetation and multipath (200Hz). Figure 29 show the process of interpolation, which is used to mach the sampling rate of rain to that of vegetation and multipath. Figure 30 shows an example of tap envelopes of the first 3 taps, which includes the combined effect of rain, vegetation and multipath.

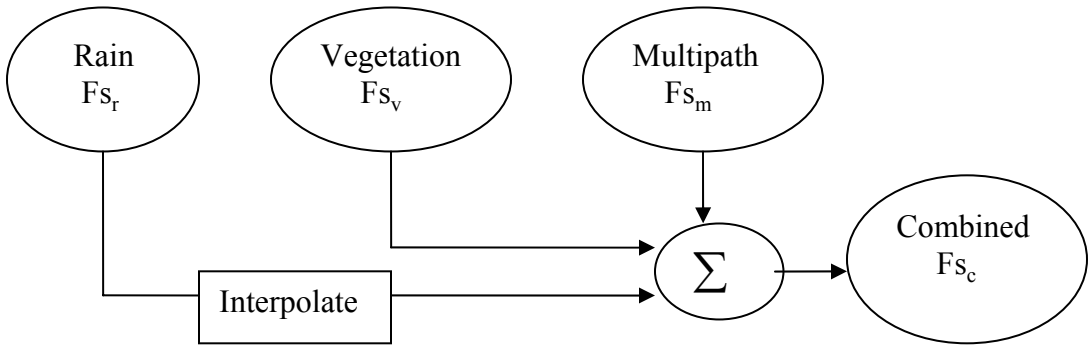

Figure 29. Rain samplings rate interpolation, where Fs_r, Fs_v, Fs_m are samplings frequency of rain, vegetation and multipath, respectively

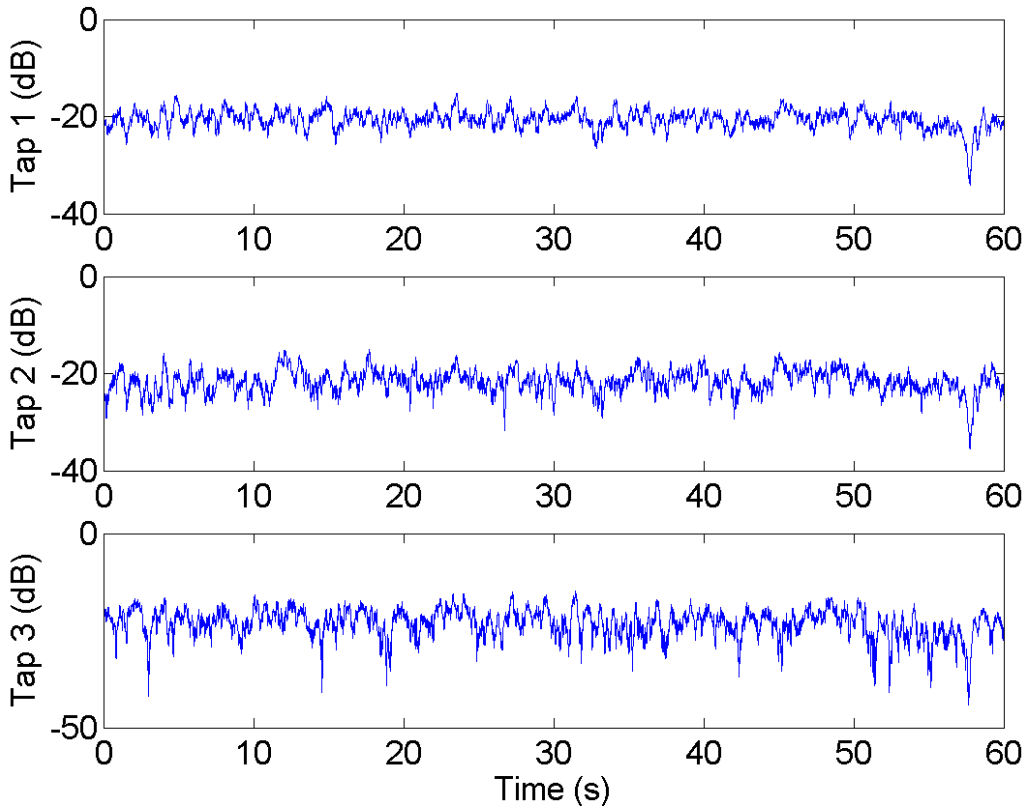

Figure 30. Tap envelopes of the first 3 taps with combined effect of rain, vegetation and multipath

In order to observe the effect of rain on multipath, Figure 31 plots the combined effect over a range of few minutes. It is shown in the figure that rain attenuation reaches its maximum value at about 4.45 minutes with an attenuation of about 13 dB. This is clearly shown in figure 31 with a deep fade at about 4.45 minutes.

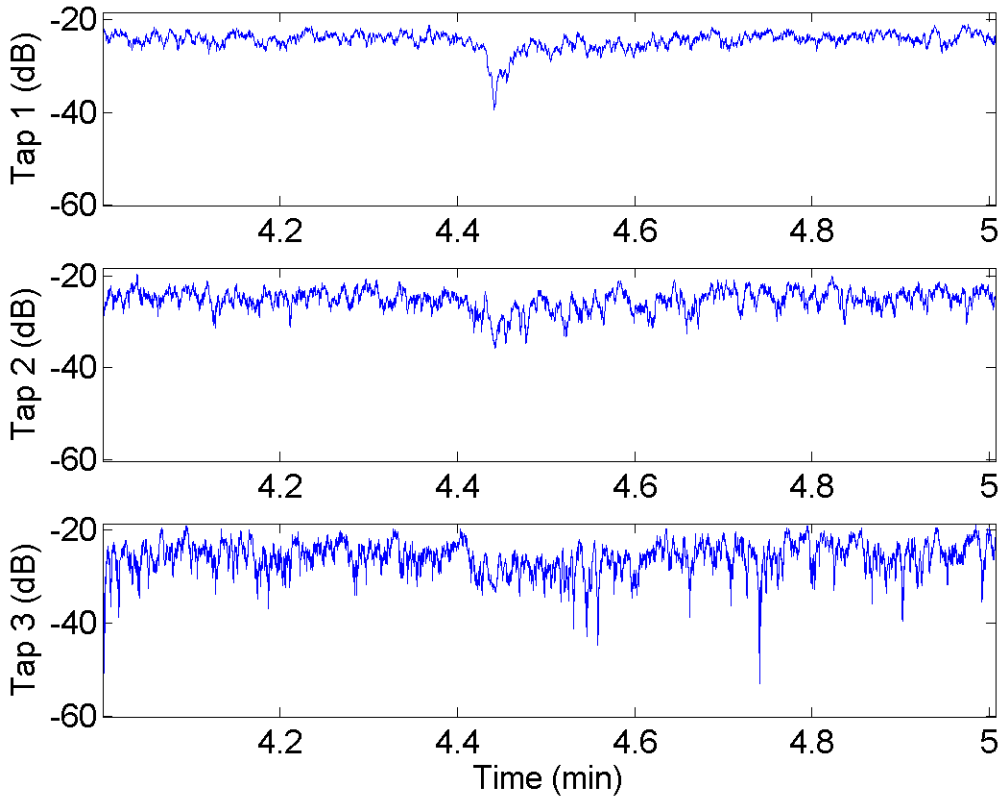

Figure 31. Tap envelopes of the first 3 taps with combined effect of rain, vegetation and multipath

7 Conclusion

BFWA systems are an effective first kilometre solution for broadband services to residential and business customers. Due to the large bandwidth available in systems operating above 20 GHz users can be offered bit rates in the order of several hundred Mbit/s, making in terms of capacity such radio links an alternative to optical fibre in many cases. However at this frequency range signals are more sensitive to propagation degradation due to rain and vegetation, and the wideband signals are susceptible to frequency selective fading due to multipath propagation. Thus a realistic channel model that accounts the effect of rain, vegetation and multipath is necessary for simulating interference mitigation and capacity enhancing techniques.

This master thesis presents a dynamic channel model for BFWA systems operating above 20 GHz. The model combines the effect of rain, vegetation and multipath to give one realistic dynamic channel model. The Maseng-Bakken statistical dynamic model of rain attenuation was adapted to model the rain attenuation. The dynamic vegetation effect was modelled as Nakagami-Rice distribution with *K*-factor depending on wind speed. A generic tapped delay line model was developed in order to characterise the multipath property of the channel. The number of taps depends on the signal bandwidth and maximum tap delay, which in turn depends on the type of environment (urban, suburban and rural) and the type of transceiver antennas (sector or omni-directional antenna). The results of this master thesis will be published and presented at 3rd international workshop, COST 280, Propagation Impairments Mitigation for Millimetre-Wave Radio Systems 6th - 8th June 2005, Prague, Czech Republic, the published paper is found in appendix A.

Future works should include the effect of scintillation in the combined model. In addition, the effect of antenna directivity on multipath property of the channel should be accounted for. This can be done by weighting each tap according to receiving antenna gain depending on angle of arrival of taps. Time clustering of the components arrival times is another area that requires further study.

Acknowledgements

In relation to this thesis I would especially like to express my gratitude for Lars Erling Bråten for his help and gaudiness. I have thoroughly enjoyed being a student of his, I have learned a great deal and have expanded my spectrum of knowledge far beyond with in communication system. I would also like to thank Terje Tjelta and Magne Petersen for their help and co-operation. I also like to thank Pål Orten, David O. A. Ojelade and the staff and researches of Telenor R&D for their help and co-operation. This thesis is based on work in the project BROADWAN (www.broadwan.org), partly funded under the Information Society Technologies (IST) priority of the European Commission Sixth Framework Programme.

References

[1] P. Soma, L. Cheun, S. Sun and M.Y. W. Chia, **"**Propagation measurements and modelling of LMDS radio channel in Singapore," IEEE Trans. Veh. Techn., vol. 52, no. 3, pp. 595-606, May 2003.

[2] T. Maseng and P. Bakken, "A stochastic dynamic model of rain attenuation," IEEE Trans. Comm., vol. 29, pp. 660 – 669, 1988.

[3] Boris Christian, Miodrag Filip, "Spatio-temporal rain Attenuation model for application to fade mitigation techniques," IEEE Trans. Ant. Prop., vol. 52, pp. 1245 – 1256, May 2004.

[4] M. H. Hashim and S. Stavrou, "Dynamic impact characterization of vegetation movements on radiowave propagation in controlled environment," Ant. Wireless Prop. Letters, vol. 2, pp. 316-318, 2003.

[5] N. Naz and D. D. Falconer, "Temporal variations characterization for fixed wireless at 29.5 GHz," In Proc. IEEE Veh. Tech. Conf., Tokyo, vol. 3, pp. 2178-2182, 15-18 May 2000.

[6] IEEE 802.16, Air Interface for Fixed Broadband Wireless Access Systems, December 2001.

[7] J. Clerk Maxwell, "A Dynamical Theory of the Electromagnetic Field," Scientific Paper, 1865, reprinted by Dover, New York, 1952.

[8] P. Mohana Shankar, Introduction to wireless Systems, John Wiley & Sons Ltd, The Atrium, Southern Gate, Chichester, West Sussex PO19 8SQ, England, ISBN: 0-471-32167-2, 2002.

[9] Simon R. Saunders, Antennas and Propagation for wireless communication Systems, John Wiley & Sons Ltd, The Atrium, Southern Gate, Chichester, West Sussex PO19 8SQ, England, ISBN: 0471986097, 1999.

[10] K. V Ravi, P. Soma, "Modeling of Local Multipoint Distribution Service (LMDS) Channel at 27.4 GHz millimeter wave band," Centre for Wireless Communications The National University of Singapore; Microwave Conference, Asia Pacific, vol. 3, pp. 702-705, 1999.

[11] Philip A. Bello, "Characterization of randomly time-variant linear channels," IEEE Trans. Comm., vol. 11, no. 4, pp. 360-393, December 1963.

[12] Cyril-Daniel Iskander, "Analytical Level Crossing Rates and Average Fade Durations for Diversity Techniques in Nakagami Fading Channels," IEEE Trans. Comm., vol. 50, no. 8, pp. 1301 – 1309, August 2002.

[13] Harry R. Anderson, Fixed broadband wireless system design, John Wiley & Sons Ltd, The Atrium, Southern Gate, Chichester, West Sussex PO19 8SQ, England, ISBN 0-470-84438-8, 2003.

[14] P. Soma, Y. W. M. Chia and L. C. Ong, "Recommendation on Time Varying Radio Propagation Channel Models and study of System Performance for LMDS," Published at http://www.ieee802.org/16/phy/contrib/802161pc-00_24.pdf, March 2000.

[15] P. B. Papazian, G. A. Hufford, and R. J. Achatz, "Study of the local multipoint distribution service radio channel," IEEE Trans. Broad., vol 43, pp 175-184, 1997.

[16] W. Zhang and N. Moayeri, "Recommendation on Channel Propagation Model for Local Multipoint Distribution Service," Document number IEEE 802.16.1pc-00/16, presented at Session #6 IEEE 802.16.2 meeting, Albuquerque, New Mexico, 6-9 March, 2000.

[17] David Falconer, "Multipath measurements and modeling for fixed broadband wireless systems in a residential environment," Document Number IEEE 802.16pc-00/01, presented at Session # 5 IEEE 802.16.1 Meeting, Richardson, TX, January 10-14, 2000.

[18] C. Briso-Rodriguez, M. A. Vazquez-Castro and J. I. Alonso-Montes, "28 GHz LMDS channel measurements and modelling for parameterised urban environments," IEEE MTT-S International, pp. 2207–2210, 2001.

[19] Y. Scott and W. Hamilton, "Propagation measurements at 28 GHz to investigate the performance of local multipoint distribution service (LMDS)," IEEE Global Telecommunications Conference, vol. 1, pp. 754-757, 1995.

[20] ACTS Project 215, Cellular Radio Access for Broadband Services, CRABS, Deliverable D3P1B, "Propagation planning procedures for LMDS," November 1998. Available from URL: http://www.telenor.no/fou/prosjekter/crabs/

[21] H. Xu, T. Rappaport, R. J. Boyle and J. H. Schaffner, “Measurements and models for 38-GHz point-to-multipoint radio wave propagation,” IEEE J. Sel. Areas Comm., vol. 18, pp. 310-321, Mars 2000.

[22] Wei Zhang, “Recommendation on Channel Propagation Model for Local Multipoint Distribution Service,” Published at http://ieee802.org/16, February 2000.

[23] K. V. Ravi, D. Guo, K. L. Cheah, ”Performance evaluation of an OFDM-based LMDS using measured channel models,” IEEE Wireless Communication and Networking Conference, no. 1, pp. 1511-1515, September 2000.

[24] K. V. Ravi and P. Soma, “Impulse Response Measurements of Local Multipoint Distribution Service (LMDS) Channel in Singapore,” IEEE ICC, no. 1, pp. 521-525, June 2000.

[25] Recommendation ITU-R P.833-4, “Attenuation in vegetation,” Geneva 2004.

[26] Recommendation ITU-R P.526-7, ”Propagation by diffraction,” Geneva, 2001.

[27] N. Currie, F. Dyer, E. Martin, “Millimetre Foliage penetration Measurements,” IEEE AP-S International Symposium, pp. 575 – 578, October 1976.

[28] D. A. J. Pearce, A. G. Burr and T. C. Tozer, “Modelling and predicting the fading performance of fixed radio links through vegetation,” In Proc. Ant. Prop., pp. 263-266, 31 March-1 April 1999.

[29] M. Polo Chavero, V. Ramos and F. Marti, “Impact of vegetation on the performance of 28 GHz LMDS transmission,” IEEE MTT-S International, vol. 3, pp. 1063 – 1066, 13-19 June 1999.

[30] A. Kajiwara, “LMDS radio channel obstructed by foliage,” In Proc. IEEE ICC, vol. 3, pp. 1583 – 1587, June 2000.

[31] S. Perras, L. Bouchard, “Fading characteristics of RF signals due to foliage in frequency bands from 2 to 60 GHz,” Wireless Personal Multimedia Communications, vol. 1, pp. 267 - 271, 27-30 October 2002.

[32] Recommendation ITU-R P.1410-2, “Propagation data and prediction methods required for the design of terrestrial broadband millimetric radio access systems operating in a frequency range of about 20-50 GHz,” Geneva, 2003.

[33] J. Maurer, D. Didascalou, V. Engels and W. Wiesbeck, “Wideband wave propagation measurements for local multipoint distribution services (LMDS) at 26 GHz,” IEEE Veh. Tech. Conf., vol. 4, pp. 1902 – 1908, 2000.

[34] Recommendation ITU-R P.530-10, “Propagation data and prediction methods required for the design of terrestrial line-of-sight systems,” Geneva, 2001.

[35] Recommendation ITU-R P.838-1, “Specific attenuation model for rain for use in prediction methods,” Geneva, 1999.

[36] Recommendation ITU-R P.841- 4, “Conversion of annual statistics to worst-month statistics,” Geneva, 2005.

[37] S. H. Lin, “Statistical behaviour of rain attenuation,” Bell Syst. Tech. J., vol. 52, pp. 557 – 581, April 1993.

[38] L. E. Bråten and W. Åsen, “Prediction of Time Dynamic Rain Attenuation at Millimetre Wavelengths,” Proc. AP2000 Millennium Conference on Antenna and Propagation, Davos, Switzerland, April 9 – 14 2000.

[39] J. P. DeCruyenaera and D. Falconer, “A shadow model for prediction of coverage in fixed terrestrial wireless systems,” In Proc. Veh. Tech. Conf., vol. 3, pp. 1427-1433, 19-22, Sept. 1999.

[40] K. Schwering, E. J. Violette, R. H. Espeland, “Millimeter-wave propagation invegetation: experiments and theory,” IEEE Trans. Geoscience and Remote Sen., vol. 26, Issue 3, pp. 355-367, May 1988.

[41] N. C. Rogers et al., “A generic model of 1 - 60 GHz radio propagation through vegetation – final report,” Qinetiq, May 2002. Available from URL: http://www.ofcom.org.uk/static/archive/ra/topics/research/topics/propagation/vegetation/vegetation-finalreportv1_0.pdf

[42] S. W. Wales,”Channel modelling and equalisation techniques for broadband mobile communications at 60 GHz,” IEE Colloquium on Methods of Combating Multipath, pp. 7/1-7/8, 26 Jan 1990.

List of abbreviations

ACF	Autocorrelation function
AFD	Average fade duration
BER	Bit error rate
BFWA	Broadband fixed wireless access
BRAN	Broadband radio access network
BS	Base station
CCDF	Complementary cumulative density function
CDF	Cumulative density function
CPE	Customer premise equipment
CRABS	Cellular Radio Access for Broadband Services
DVB-RCS	Digital video broadcasting with return channel via satellite
DSL	Digital subscriber link
EM	Electromagnetic
ETSI	European telecommunications standards institute
FIR	Finite impulse response
FSO	Free space optic
FTTH	Fibre to the home
HFC	Hybrid fibre coaxial
IR	Impulse response
MAC	Medium access control layer
MIMO	Multiple input multiple output
MMSE	Minimum means square error
LAN	Local area network
LCR	Level crossing rate
LMDS	Local multipoint distribution service
LOS	Line of sight
PDF	Probability density function
PDP	Power delay profile
PLC	Power line communication
PTM	Point to multipoint
PTP	Point to point
PHY	Physical layer
QAM	Quadrate amplitude modulation
RF	Radio frequency
SNR	Signal to noise ratio
TDD	Time division duplex
WLAN	Wireless local area network
WSSUS	Wide sense stationary uncorrelated scattering

Appendix A. Paper to COST Action 280

COST Action 280

"Propagation Impairment Mitigation for Millimetre Wave Radio Systems"

Time dynamic channel model for broadband fixed wireless access systems

Michael Cheffena[1)], Lars Erling Bråten [2)], Terje Tjelta[2)]

1) UniK - University Graduate Center, N-2007 Kjeller, Norway. michaec@ulrik.uio.no
2) Telenor R&D, Access Networks, N-1331 Fornebu. {lars-erling.braten, terje.tjelta}@telenor.com

Abstract

Broadband fixed wireless access (BFWA) systems have been recognized as an effective first kilometer solution for broadband services to residential and business customers. The large bandwidths available in frequency bands above 20 GHz, makes radio systems with very high capacities possible. Users can be offered bit rates in the order of several hundred Mbit/s, making in terms of capacity such radio links an alternative to optical fibre in many cases. In addition wireless always offers the freedom of broadband being away from the fixed access point. The objective of this study is to develop a realistic time dynamic channel model for BFWA operating above 20 GHz and utilising adaptive physical layer techniques. The channel model developed represents the time varying wideband channel impulse response including degradations due to multipath propagation, rain attenuation, and vegetation fading. The channel model is suitable for simulating mitigation techniques for interference between base stations as well as adaptive modulation and coding techniques.

1. Introduction

BFWA may be divided between systems that operate below 20 GHz and systems that operate above 20 GHz. For systems operating above 20 GHz, there are available wide bandwidths for delivering broadband services such as video, audio and data. In addition, a high frequency reuse is possible, and the size of radiating and receiving antennas and electronic components is reduced compared to lower frequency systems. However, mm-wave signals are more sensitive to propagation degradation due to rain and vegetation, and the wideband signals are susceptible to frequency selective fading due to multipath propagation. Thus a realistic channel model that accounts the effect of rain, vegetation and multipath is necessary for simulating interference mitigation and capacity enhancing techniques. In the literature, a propagation study for BFWA systems has been reported in [1], where multipath, signal attenuation, depolarisation, and cell-to-cell coverage were studied. Based on measurements conducted at 27.4 GHz, static and dynamic wideband

channel model for BFWA were developed [2]. Dynamic models for rain attenuation are reported in for example [3] and [4]. There are a number of studies on the dynamic effects of vegetation; among them [5] and [6]. In this paper we present a wideband statistical channel model which combines the effect of precipitation, vegetation and multipath propagation, see Fig. 1.

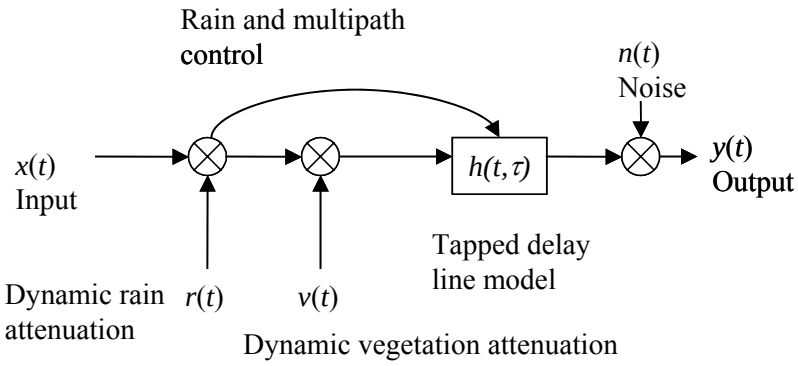

Figure 1. Time dynamic BFWA channel model

Section 2 describes the dynamic effect of rain and the model used to represent it. In Section 3 the dynamic effect of vegetation and the developed dynamic model for vegetation effects are discussed. A generic tapped delay line model for multipath propagation is presented in Section 4. In Section 5 the combined effect of vegetation, rain and multipath is discussed, followed by conclusions. This paper is based on work in the project BROADWAN (www.broadwan.org), partly funded under the Information Society Technologies (IST) priority of the European Commission Sixth Framework Programme.

2. Time dynamic rain attenuation

Attenuation by rain occurs as a result of absorption and scattering and the dynamical variation is caused by the temporal and spatial changes of the precipitation. Rain attenuation must be accounted at frequency range of interest, and above about 10 GHz its importance increases rapidly with frequency. In the planning of communication systems, the dynamic properties of rain attenuation are also of significant interest. In the proposed combined channel model, the Maseng-Bakken statistical dynamic model of rain attenuation is adapted from [3]. The received signal attenuation α (in dB) is modelled as a log-normally distributed variable. By utilising a memoryless nonlinearity the attenuation is transformed into a stationary Gaussian process with zero mean and unit variance.

$$x(t) = \ln\left(\alpha(t)/\alpha_m\right)/\sigma_a \tag{1}$$

where σ_m is the median attenuation and σ_a the standard deviation of ln(α).The value of the average rain attenuation and standard deviation may be derived from either local measurements of attenuation distribution or estimated attenuation distribution from ITU-R Rec. P.530 [7] by applying curve-fitting routines. The mean square error of complementary cumulative distribution function (*ccdf*) of estimated rain attenuation and *ccdf* of lognormal distribution are minimised to give the best fit. The time dependence is

described by the parameter β, which is used in a first order infinite impulse response filter to shape the auto correlation function. The auto correlation function is assumed to have a relatively simple shape of a decaying exponential function corresponding to an auto regressive process of first order

$$R_{XX}(\tau) = e^{(-\beta \cdot |\tau|)} \quad (2)$$

A small value of β corresponds to slowly varying rain attenuation dynamics. An investigation reported in [4] found $3.16 \times 10^{-4} \leq \beta \leq 3.16 \times 10^{-3}$, with a central value of $\beta = 7.9 \times 10^{-3}$ s^{-1}. The variations in the results indicate that β depends on the local climate as well as the form of precipitation at one location. Previously reported values for β are $1.7\ 10^{-3}$ [3] and $1.8\ 10^{-3}$ [9]. Fig. 2 shows simulated dynamic rain attenuation with a samplings rate of 10 Hz, assuming a rain rate of 30 mm/h, resulting in an attenuation at 0.01 percent of time of 15.66 dB for a 2 km length path (estimated from ITU-R Rec. P530) with $\beta = 7.9 \times 10^{-4}\, s^{-1}$. The optimised lognormal parameters that give best fit between *ccdf* of estimated rain attenuation and *ccdf* of lognormal distribution are -4.9388 and 2.9956 for the mean and standard deviation of lognormal distribution respectively.

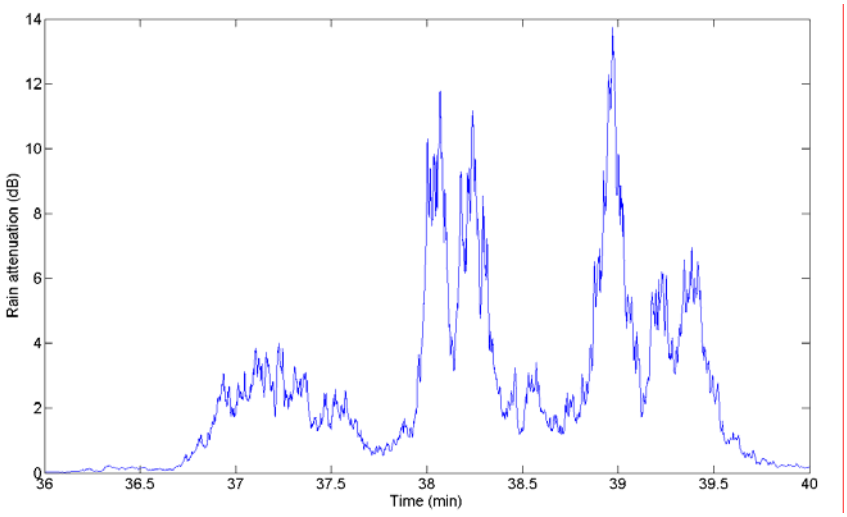

Figure 2. Dynamic rain attenuation time series

Based on the BFWA system layout, e.g. distances between transceivers, and local rain rate and rain dynamics statistics, this time dynamic rain attenuation model can be incorporated into system level simulations together with other propagation degradations such as scintillation, multipath and vegetation attenuation.

3. Dynamic vegetation effects

Vegetation effects can severely limit the performance of BFWA system operating at mm-wavelengths. Attenuation due to single trees varies significantly with species, whether trees are in leaf or wet [12]. At frequencies above 20 GHz leaves and needles have dimensions large compared to wavelength and will significantly affect the propagation conditions. A theoretical description of penetration into vegetation is given by the theory of radiative energy transfer. Range dependence of vegetation attenuation is characterised by high attenuation at short vegetation depths and a reduced attenuation rate at larger

depth due multiple scattering causing beam broadening and depolarisation [13]. The transition between the two regimes can be rather abrupt and the change in attenuation rate substantial. Due to limited power margin in operational BFWA systems, the first regime is most interesting. In this regime, the received signal consists of the coherent components attenuated direct wave, diffracted and ground reflected waves in addition to the diffuse component resulting from scattering within the foliage. Measurements reported in [14] showed that diffraction around the tree is the dominant mode of propagation for trees in leaf with only a weak scattered component. For trees without leaves the ground reflected component dominated.

It was found in [15] that the lognormal distribution gave the best fit to measurements of envelope for low attenuation values, and the extreme value distribution gave better results for the large attenuation values in the tail of the distribution. It should be noted that the Nakagami-Rice and Rayleigh distributions were tested but rejected in a χ^2. In an indoor 29.5 GHz measurement campaign reported in [16], the attenuation relatively closely followed a Nakagami-Rice distribution with *K*-factor ranging from about 0.5 to 4. A similar indoor study is reported in [17] where Nakagami-Rice, Rayleigh and Gaussian distributions were compared at 17 GHz. The best fit was obtained with a Nakagami-Rice distribution, with a *K*-factor exponentially decreasing with wind speed. In this study there existed a strong direct component, in addition to the scattered multipath component with power increasing with wind speed up to a limiting value. In a study measuring the effect of foliage at 29.5 GHz, 115 links with 10 minutes recordings were analysed including several tree species [6]. A Kolmogorov-Smirnov test was applied to rank Rayleigh, Nakagami-Rice, lognormal and Nakagami-m, resulting in 95 per cent pass for the Nakagami-Rice distribution for the envelope distribution. In a 28 GHz trial, the Kolmogorov-Smirnov test ranked the Gaussian distribution as better than Nakagami, Rayleigh and Nakagami-Rice [18].

There are significant variations between the different measurement campaigns with respect to the best choice of theoretical attenuation distribution function, however, the majority of the experimental results seem to indicate that the Nakagami-Rice distribution is suitable for general modelling usage. This implies that the coherent component propagation through, and diffracting around, the vegetation is considered constant. The PDF of the Nakagami-Rice attenuation distribution for the envelope *v* is

$$p(v) = \frac{v}{\sigma^2} e^{-\left(v^2+a^2\right)/2\sigma^2} I_0\left(\frac{va}{\sigma^2}\right) \tag{3}$$

where I_0 is the modified Bessel function of zero order. The relation between the coherent components amplitude, *a*, and the power in the diffuse component, $2\sigma^2$, may be expressed by the Nakagami-Rice factor $K = 10 \cdot \log_{10}\left(a^2 / 2\sigma^2\right)$. The average total received power can be determined from ITU Rec. P.833 on vegetation.

It was observed from 12 and 17 GHz measurements reported in [5] that the *K*-factor decreases exponentially as wind speed increases see Fig. 3b. The CRABS project reported measurements of signal level standard deviation at 42 GHz [20], leading to the linear model between standard deviation and wind speed in ITU-R Rec. 1410 [11]. The

standard-deviation produced by the Nakagami-Rice model was compared to the ITU-R P.1410 model as function of wind speed, and a good agreement was obtained between the models, see Fig. 3a. Fig. 3b shows the variation of Nakagami-Rice *K*-factor as a function of wind speed for three different frequencies. By estimating the average vegetation attenuation at 42 GHz according to ITU-R P.833 [10], and then assuming a Nakagami-Rice distributed envelope and a variation of the *K*-factor according to Fig. 3b, we get a resulting vegetation time series as shown in Fig. 4. The mean vegetation attenuation is 12.6 dB for the 42 GHz signal, the sampling rate is 200 Hz, and the dynamics of the Gaussian processes is controlled by utilising a first order Butterworth filter with a 3 dB cut-off frequency of 1.5 Hz, resulting in a 40 dB cut-off frequency of about 50 Hz, comparable to the results reported in [15], [6] and [21].

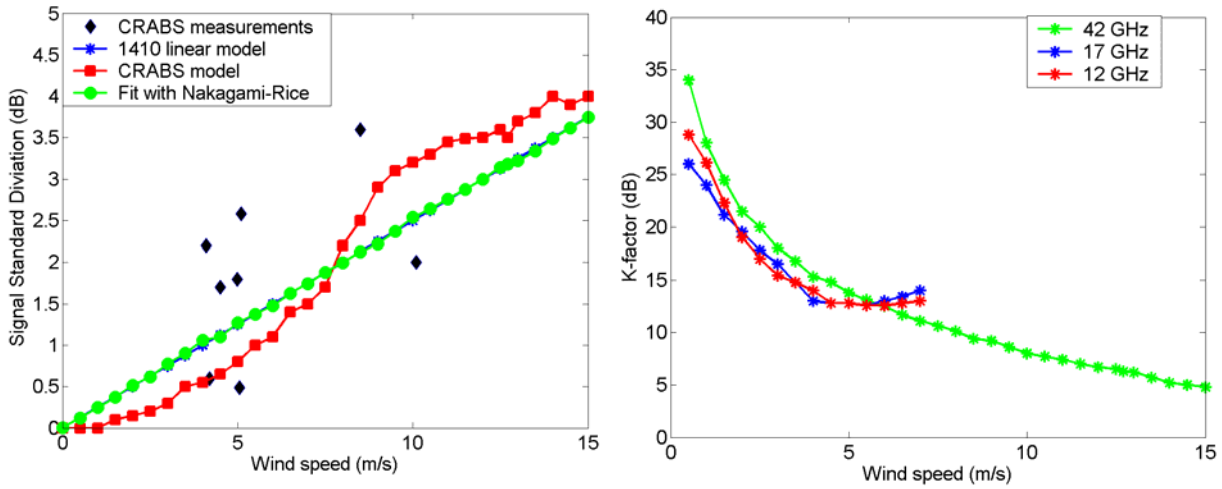

a) CRABS measurements, ITU-R P.1410 linear model and fit with Nakagami-Rice

b) *K*-factor as function of wind speed 17 and 12 GHz from [5], 42 GHz derived from Fig. 3a

Figure 3. Signal standard deviation and Nakagami-Rice K-factor as function of wind speed

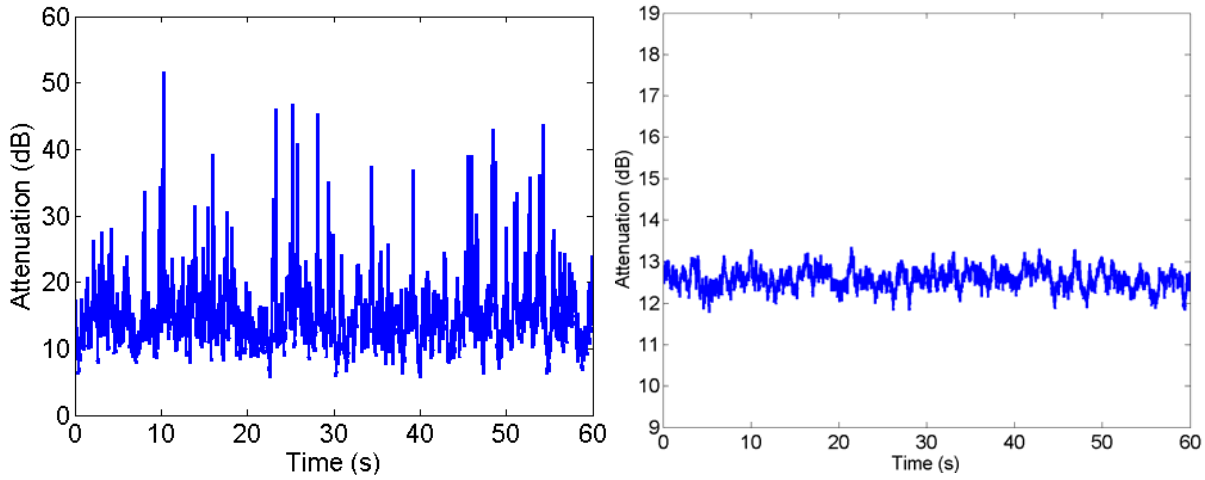

a) In leaf, $K = 3$ dB, wind speed over 15 m/s

b) In leaf, $K = 28$ dB, wind speed 1 m/s

Figure 4. Dynamic vegetation attenuation time series

4. Tapped delay line model

Multipath propagation causing frequency selective fading may become significant when the system bandwidth exceeds the channels coherence bandwidth. The time delays between the multipath components depends on both the surrounding reflectors and the antennas involved, imposing a distinction between propagation paths between base stations and propagation paths from a base station to the users. Depending on the antennas utilised, and the transmission environment, multipath components with significant delay spreads will occur. To enable interference estimation and simulations of interference reduction techniques we define the time varying channel impulse response $h(t,\tau)$:

$$h(t,\tau) = \sum_{n=0}^{N-1} m(t,n)\delta(t-\tau_n)e^{-j(\omega_c\tau_n+\varphi_n(t))} \tag{4}$$

where n is the tap index, N is the number of taps, ω_c is the carrier angular frequency, τ_n is the excess delay of each multipath component, $\varphi_n(t)$ is the phase for tap number n within the range [0, 2π], and $m(t,n)$ denotes the time varying envelope for tap number n. Normally m is normalised to obtain a unit channel gain. Wideband 200 MHz channel measurements at 38 GHz in a campus environment were reported in [19], multipath on a LOS link was only observed during rain and hail, not during clear weather. This may be due to changes in electromagnetic properties of the buildings and vegetation as the scattering surfaces becomes wet. This is supported by the increased multipath activity on the two partly obstructed paths during rain. After the surfaced dried up, the multipath power decreased. The short-term variations in signal strength over 1-2 minutes was well described by a Nakagami-Rice distribution with a Nakagami-Rice factor K depending on the rain intensity R (mm/h) [19]

$$K = 16.88 - 0.04R \qquad dB \tag{5}$$

With the tapped delay line model the Nakagami-Rice factor K becomes

$$K(t) = \frac{\max_n\left(m(t,n)^2\right)}{1-\max_n\left(m(t,n)^2\right)} \tag{6}$$

We may choose the main scattered component (specular reflection or LOS component) according to a given Nakagami-Rice factor K and let the remaining taps follow Nakagami-Rice distributions with a K factor decreasing with average tap power. In the simulations we have used ΔK = 5 dB (decrementing factor) between the taps. The path occurrence process may be modelled as a modified Poisson renewal process taking into account that paths tend to arrive in time clusters [22]. For simplicity, however, we have assumed a uniform spacing between the taps in our model. Depending on the signal bandwidth and the maximum tap delay, depending on the type of environment, the model generates taps with average tap power given by:

$$P = \exp(-3\tau_n / \tau_{\max}) \tag{7}$$

where τ_n is the tap delay and $\tau_{\max}$ is the maximum tap delay. The maximum tap delay is a random function which depends on the environment type and the type of transceiver antennas (transmitter: sector or omni-directional antenna, receiver: narrow-beam or wide-

beam antenna), measurements from [2] reported a maximum delay of 400 ns in the urban case. The dynamics is controlled by filtering the Gaussian processes, as for vegetation, and we have assumed the same filtering bandwidth and sampling frequency. The resulting power delay profile and tap time series are shown in Fig. 5.

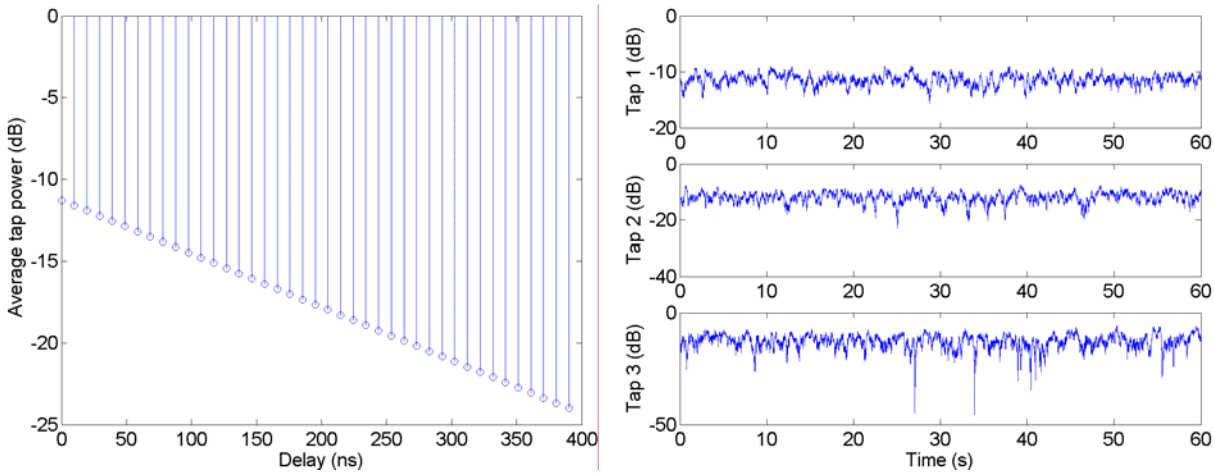

a) Power delay profile b) Tap envelopes of the first 3 tap

Figure 5. Generic tapped delay line model, with maximum tap delay of 400 ns

5. Combined dynamic channel model

The individual dynamic models for rain, vegetation and multipath are combined to give one realistic channel model, which accounts the effect of rain, vegetation and multipath as shown in Figure 1. The sampling rate of rain (10 Hz) is interpolated to be equal to sampling rate of vegetation and multipath (200 Hz). Fig. 6 shows an example of tap envelopes of the first 3 taps, which includes the combined effect of rain, vegetation and multipath.

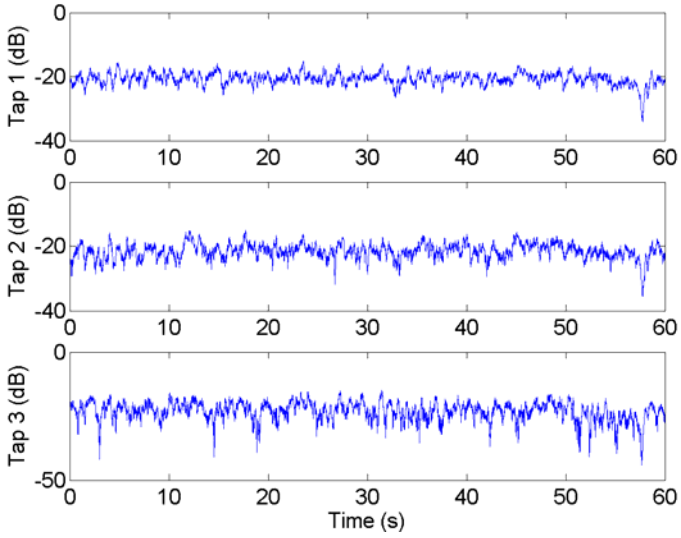

Figure 6. Tap envelopes of the first 3 taps of the combined effect

6. Conclusion

This paper presents a dynamic channel model for BFWA. The model combines the effect of rain, vegetation and multipath to give one realistic dynamic channel model. Maseng-Bakken statistical dynamic model of rain attenuation was adapted to model the rain attenuation. The dynamic vegetation effect was modelled as Nakagami-Rice distribution with *K*-factor depending on wind speed. A generic tapped delay line model was developed, in which the number of taps depend on maximum tap delay.

Future works should include the effect of scintillation in the combined model. In addition, the effect of antenna directivity on multipath property of the channel should be accounted for. Time clustering of the components arrival times is another area that requires further study.

References

[1] P. B. Papazian, G. A. Hufford and R. J. Achatz, "Study of the local multipoint distribution service radio channel," IEEE Trans. Broad., vol. 43, pp. 175 – 184, 1997.

[2] P. Soma, L. Cheun, S. Sun and M. Y. W. Chia, "Propagation measurements and modelling of LMDS radio channel in Singapore," IEEE Trans. Veh. Techn., vol. 52, no. 3, pp. 595 – 606, May 2003.

[3] T. Maseng and P. Bakken, "A stochastic dynamic model of rain attenuation," IEEE Trans. Comm., vol. 29, pp. 660 – 669, 1988.

[4] B. Christian, M. Filip, "Spatio-temporal rain Attenuation model for application to fade mitigation techniques," IEEE Trans. Ant. Prop., vol. 52, pp. 1245 – 1256, May 2004.

[5] M. H. Hashim and S. Stavrou, "Dynamic impact charcterization of vegetation movements on radiowave propagation in controlled environment," Ant. Wireless Prop. Letters, vol. 2, pp. 316-318, 2003.

[6] N. Naz and D. D. Falconer, "Temporal variations characterization for fixed wireless at 29.5 GHz," In Proc. Veh. Tech. Conf., Tokyo, vol.3, pp. 2178-2182, 15-18 May 2000.

[7] Recommendation ITU-R P.530-10,"Propagation data and prediction methods required for the design of terrestrial line-of-sight systems," Geneva, 2001.

[8] S. H. Lin, "Statistical behavior of rain attenuation", Bell Syst. Tech.J., vol 52, pp 557 – 581, April 1993.

[9] A. Burgueno, E. Vilar and M. Puigcerver, "Spectral Analysis of 49 Years of Rainfall Rate and Relation to Fade Dynamics", IEEE Trans. Comm.,vol. 38, pp. 1359-1366, Sept 1990.

[10] Recommendation ITU-R P.833-4, "Attenuation in vegetation," Geneva 2004.

[11] Recommendation ITU-R P.1410-2, "Propagation data and prediction methods required for the design of terrestrial broadband millimeter radio access systems operating in a frequency range of about 20-50 GHz in vegetation," Geneva 2003.

[12] J. P. DeCruyenaera and D. Falconer, "A shadow model for prediction of coverage in fixed terrestrial wireless systems," In Proc.Veh. Tech. Conf., vol. 3, pp. 1427-1433, 19-22, Sept. 1999.

[13] F. K. Schwering, E. J. Violette, R. H. Espeland, "Millimeter-wave propagation invegetation: experiments and theory," IEEE Trans. Geoscience and Remote Sen., vol. 26, Issue 3, pp. 355-367, May 1988.

[14] N. C. Rogers et al., "A generic model of 1-60 GHz radio propagation through vegetation – final report," Qinetiq, May 2002. Available from URL: www.ofcom.org.uk/static/archive/ra/topics/research/topics/propagation/vegetation/vegetation-finalreportv1_0.pdf

[15] S. Perras, L. Bouchard, "Fading characteristics of RF signals due to foliage in frequency bands from 2 to 60 GHz," Wireless Personal Multimedia Communications, vol. 1, pp. 267 - 271, 27-30 Oct. 2002.

[16] A. Kajiwara, "LMDS radio channel obstructed by foliage," In Proc. IEEE ICC, vol. 3,pp. 1583-1587, 18-22 June 2000.

[17] M. H. Hashim and S. Stavrou, "Dynamic impact characterization of vegetation movements on radiowave propagation in controlled environment," Ant. Wirel. Prop. Letters, vol. 2, pp. 316-318, 2003.

[18] M. Chavero, V. Polo, F. Ramos and J. Marti, "Impact of vegetation on the performance of 28 GHz LMDS transmission," In Proc. Microwave Symposium Digest, IEE MTT-S, vol. 3, pp. 1063-1066, 13-19 June 1999.

[19] H. Xu, T. Rappaport, R. J. Boyle and J. H. Schaffner, "Measurements and models for 38-GHz point-to-multipoint radiowave propagation," IEEE J. Sel. Areas Comm., vol 18, no. 3, pp. 310-320, March 2000.

[20] ACTS Project 215, Cellular Radio Access for Broadband Services, CRABS, Deliverable D3P1B, "Propagation planning procedures for LMDS", Nov. 1998. Available from URL: www.telenor.no/fou/prosjekter/crabs/.

[21] D. A. J. Pearce, A. G. Burr and T. C. Tozer, "Modelling and predicting the fading performance of fixed radio links through vegetation," In Proc. Ant. Prop., pp. 263-266, 31 March-1 April 1999.

[22] S. W. Wales, "Channel modelling and equalisation techniques for broadband mobile communications at 60 GHz," IEE Colloquium on Methods of Combating Multipaths, pp. 7/1-7/8, 26 Jan 1990.